ENSO in the CMIP5 Simulations: Life Cycles, Diversity, and Responses to Climate Change

CHEN CHEN AND MARK A. CANE

Lamont-Doherty Earth Observatory of Columbia University, Palisades, New York

ANDREW T. WITTENBERG

NOAA/Geophysical Fluid Dynamics Laboratory, Princeton, New Jersey

DAKE CHEN

State Key Laboratory of Satellite Ocean Environment Dynamics, Second Institute of Oceanography, Hangzhou, China, and Lamont-Doherty Earth Observatory of Columbia University, Palisades, New York

(Manuscript received 18 December 2015, in final form 6 October 2016)

ABSTRACT

Focusing on ENSO seasonal phase locking, diversity in peak location, and propagation direction, as well as the El Niño–La Niña asymmetry in amplitude, duration, and transition, a set of empirical probabilistic diagnostics (EPD) is introduced to investigate how the ENSO behaviors reflected in SST may change in a warming climate.

EPD is first applied to estimate the natural variation of ENSO behaviors. In the observations El Niños and La Niñas mainly propagate westward and peak in boreal winter. El Niños occur more at the eastern Pacific whereas La Niñas prefer the central Pacific. In a preindustrial control simulation of the GFDL CM2.1 model, the El Niño–La Niña asymmetry is substantial. La Niña characteristics generally agree with observations but El Niño's do not, typically propagating eastward and showing no obvious seasonal phase locking. So an alternative approach is using a stochastically forced simulation of a nonlinear data-driven model, which exhibits reasonably realistic ENSO behaviors and natural variation ranges.

EPD is then applied to assess the potential changes of ENSO behaviors in the twenty-first century using CMIP5 models. Other than the increasing SST climatology, projected changes in many aspects of ENSO reflected in SST anomalies are heavily model dependent and generally within the range of natural variation. Shifts favoring eastward-propagating El Niño and La Niña are the most robust. Given various model biases for the twentieth century and lack of sufficient model agreements for the twenty-first-century projection, whether the projected changes for ENSO behaviors would actually take place remains largely uncertain.

1. Introduction

ENSO behaviors in observations and models have shown rich diversity and asymmetry. El Niños can peak at both the eastern Pacific (EP) and the central Pacific (CP) (e.g., Larkin and Harrison 2005; Ashok et al. 2007; Weng et al. 2007; Kao and Yu 2009; Kug et al. 2009; Taschetto and England 2009; Lee and McPhaden 2010; Newman et al. 2011; Takahashi et al. 2011; Karnauskas 2013; Capotondi et al. 2015; Fedorov et al. 2015; D. Chen et al. 2015). Extreme El Niños propagate eastward whereas moderate El Niños and La Niñas tend to propagate westward (Fedorov and Philander 2001; McPhaden and Zhang 2009; Lengaigne and Vecchi 2010; Santoso et al. 2013; Kim and Cai 2014). Asymmetries between El Niño and La Niña have also been documented; for example, El Niños often have larger amplitude than La Niñas, La Niñas are more durable than El Niños, and La Niñas often tightly follow extreme El Niños but not vice versa (Kang and Kug 2002; Larkin and Harrison 2002; An and Jin 2004; Schopf and Burgman 2006; Ohba and Ueda 2009; Frauen and Dommenget 2010; Okumura et al. 2011; Choi et al. 2013; Dommenget et al. 2013). ENSO phase-locked to the end of the calendar year has been found to be the outcome of several feedbacks and is subject to

Corresponding author e-mail: Chen Chen, cchen@ldeo.columbia.edu

DOI: 10.1175/JCLI-D-15-0901.1

change when these competing influences change (e.g., Tziperman et al. 1995, 1997, 1998; Neelin et al. 2000; An and Wang 2001; Xiao and Mechoso 2009).

Detailed ENSO behaviors matter for ENSO teleconnection and impacts. For example, El Niños peaking at the central or eastern Pacific have been shown to have varying impacts on the U.S. winter air temperature and precipitation (Yu et al. 2012). Details of the El Niño to La Niña transition (e.g., whether El Niños persist longer or rush to the La Niña phase) have been linked to varying likelihoods of U.S. regional tornados in the spring (Lee et al. 2016).

Usually, an individual ENSO behavior is investigated separately. To reach a large picture understanding, a comprehensive measure of various ENSO behaviors is required. In this study we introduce a set of empirical probabilistic diagnostics (EPD) to efficiently calculate the statistics for various ENSO behaviors, including ENSO seasonal phase locking, diversity in peak location and propagation direction, and El Niño–La Niña (EN–LN) asymmetry in amplitude, duration, and transition. These diagnostics are first applied to the observed SST data and the results agree with many previous understandings, indicating that this new diagnostic framework is valid. One recent research focus concerns ENSO in a changing climate (e.g., Collins et al. 2010; Cai et al. 2015a). Therefore, after characterizing the various ENSO behaviors over the past ~150 years, we then assess how ENSO behaviors will vary and change in the warming climate.

ENSO varies from century to century, not only in amplitude and frequency (Wittenberg 2009) but also in its diversity and asymmetry characteristics. For example, in the past 100-yr epoch, El Niños have mainly peaked at the eastern Pacific. In the most recent decade El Niños have more often peaked at the central Pacific (Lee and McPhaden 2010). So the following questions arise: In the warming twenty-first century, will El Niños switch to more often peak at the central Pacific? If this change does happen, is it necessarily a result of the changing forcing, or could it be merely a natural variation? Newman et al. (2011) and Yeh et al. (2011) have suggested that more occurrences of the central Pacific El Niño in the recent decade may be simply a part of the natural variation.

Given only ~150 years of observation, how can we estimate the natural variation of each ENSO behavior? All the aspects of ENSO behaviors are dynamically linked, so we apply the following two approaches to ensure a coherency between the estimates of each ENSO behavior. The first approach is using a long control simulation of a coupled GCM under a constant forcing without a trend. Here a 4000-yr preindustrial simulation from the GFDL CM2.1 coupled GCM (Delworth et al. 2006) is analyzed as one example. A second approach is using a long stochastic forced simulation of a data-driven model. A 4000-yr simulation from an empirical model reduction (EMR) (Kravtsov et al. 2005; Kondrashov et al. 2005, 2015; Chen et al. 2016) is analyzed as one example. Compared to GFDL CM2.1, EMR shows a slightly better overall performance for nine aspects of ENSO behavior, and therefore we mainly use EMR to estimate how these ENSO behaviors may vary without a changing forcing.

As to ENSO's response to the warming climate, it may be reflected not only in its amplitude but also in other ENSO characteristics. Here we mainly focus on SST climatology, ENSO amplitude, annual cycle, and nine aspects from EPD. We analyze 37 models from phase 5 of the Climate Model Intercomparison Project (CMIP5) to investigate the following questions: If the models suggest that ENSO behavior will change significantly in the twenty-first century? Do models agree on this change? Are the projected changes in ENSO behaviors more response to the changing forcing or mainly part of the natural variation? Since EPD measures various ENSO characteristics, we then have an opportunity to investigate which aspects are most responsive to the trend forcing and which aspects vary most so that the forced changes cannot be easily distinguished from the range of the natural variation.

All estimates, no matter whether for the natural variation or the forced change of ENSO behavior, have to be based on model simulations, so in this study EPD is carried out with two purposes. The first is to assess ENSO's variation and change and the second is to diagnose model performance and biases with regard to ENSO behaviors. When we analyze the GFDL CM2.1 and EMR models, we briefly investigate how the model biases with regard to ENSO behavior may be related to the model nonlinearity. When we assess the CMIP5 models, we investigate whether models are able to represent ENSO behavior realistically for the twentieth century and thus whether they are likely to reliably project behavior in the twenty-first century. We also briefly investigate how the models' biases with regard to ENSO behaviors may be related to the model biases pertaining to the mean state.

2. Data

a. *Observations*

The 1870–present monthly HadISST v1.1 (Rayner et al. 2003) and 1850–present monthly COBE[1] v2

[1] Centennial in Situ Observation-Based Estimates of the Variability of SST and Marine Meteorological Variables.

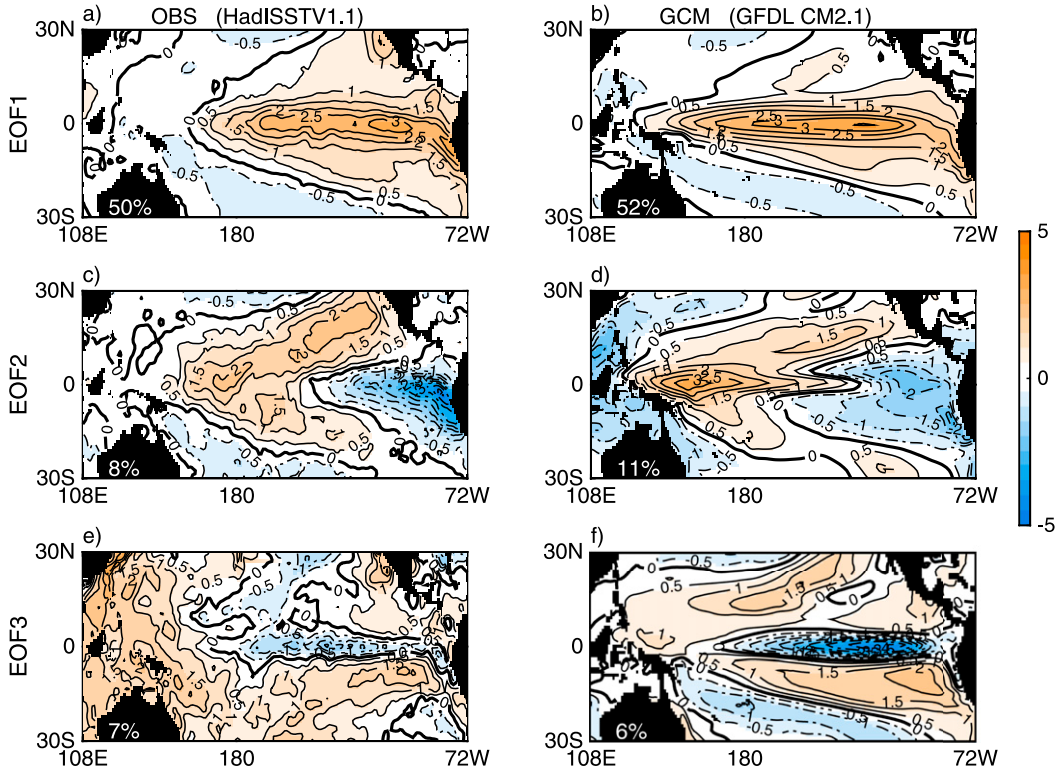

FIG. 1. The first three normalized EOF patterns of tropical Pacific SSTA in (left) OBS (1870–present monthly HadISST v1.1) and (right) GCM (4000-yr monthly GFDL CM2.1 preindustrial control run). Positive (negative) values are shown in solid (dashed) contours. The zero value is highlighted in the thick solid contour.

(Hirahara et al. 2014) datasets have relatively high spatial resolution (1° × 1°) and capture the diversity of ENSO behaviors. The results using COBE are overall consistent with HadISST, so only the HadISST results, referred to as OBS, are shown hereafter. Tropical Pacific (30°S–30°N, 108°E–72°W) SST anomalies (SSTA) are calculated by removing the monthly climatology based on the commonly used 1950–2010 period. A linear detrending is applied on the SSTA at each grid point to remove the global warming trend. Then a 3-month running average is applied to the SSTA to smooth the temporal noise.

Leading modes of SST variability in the tropical Pacific region are depicted using empirical orthogonal function (EOF) analysis (Fig. 1). The leading EOF shows the classic El Niño pattern, which is the dominant variability explaining 50% of the total variance in the tropical Pacific. The second EOF shows a zonal dipole pattern with a positive loading in the western Pacific and a negative loading in the eastern Pacific, which adds a central Pacific or eastern Pacific "flavor" to the main El Niño pattern and explains 8% of the total variance. Following the idea in the previous studies (e.g., Ashok et al. 2007; Takahashi et al. 2011), the first two EOF modes and their principal components (PCs) are used to categorize ENSO diversity in the central or eastern Pacific. Takahashi et al. (2011) showed that using PC1/PC2 as a basis is equivalent to many other indices used to define EP/CP behavior. Details are given in the methods section.

The third EOF depicts an equatorial cooling and extra-equatorial warming that is similar to the equatorial ocean dynamic thermostat pattern (Clement et al. 1996; Cane et al. 1997; Solomon and Newman 2012). EOF3 explains 7% of the total variance. Its eigenvalue appears not well separated from EOF2 (8%) in the observations. The sensitivity tests show that EOF1 and EOF2 are robust modes in that their PCs are not as greatly influenced by the varying climatology as EOF3/PC3, which has significant multidecadal variability. When we filter out low frequencies (>40-yr periods) in the original data, the eigenvalue of EOF3 (5%) is then well separated from EOF2 (9%).

b. *Coupled GCM: GFDL CM2.1*

Nature only provides one realization, so the limited record of SST observations is an obstacle to investigating the variation of ENSO behavior on a century scale.

Therefore, long simulations of coupled intermediate models such as the Zebiak–Cane (ZC) model (Zebiak and Cane 1987) and a fully coupled GCM with fixed external forcing are often used to investigate the natural variation of ENSO (e.g., Cane et al. 1995; Wittenberg 2009; Yeh et al. 2011).

Here we analyze a 4000-yr monthly control simulation from the GFDL CM2.1 coupled GCM (Delworth et al. 2006) with the forcings, including solar irradiance, land cover, and atmospheric composition fixed at preindustrial (1860) values. This simulation has been analyzed in various ENSO studies (e.g., Wittenberg et al. 2006; Wittenberg 2009; Kug et al. 2010; Xie et al. 2010; Choi et al. 2013; Karamperidou et al. 2014; Wittenberg et al. 2014) and is shown to have a reasonable ENSO performance although with a too strong amplitude and too little seasonal synchronization. This simulation is referred to simply as ''GCM'' hereafter.

Tropical Pacific (30°S–30°N, 108°E–72°W) SSTA values are calculated by removing the monthly climatology based on the full length of the record. A linear detrending and a 3-month running average are applied. EOF analysis is then performed. The leading three EOFs from GCM respectively explain 52%, 11%, and 6% of the total variance in the tropical Pacific. GCM EOF patterns are overall consistent with OBS (Fig. 1), although slightly shifted west and narrower in the meridional direction as shown in Wittenberg et al. (2006).

c. Data-driven modeling: EMR

Since every coupled model has its own ENSO behavior that is to some extent biased away from the current climate, the natural variation of ENSO estimated by an individual GCM may be model dependent. Long stochastically forced simulations from a data-driven model offer an alternative approach. The model dynamics are fit from the observations, thus assuring that at least some of the statistics and features of the simulated ENSO resemble the observed ENSO closely.

Here we apply the empirical model reduction framework (e.g., Kravtsov et al. 2005; Kondrashov et al. 2005, 2015; Chen et al. 2016). It is a regression model with quadratic nonlinearities constructed in a reduced EOF phase space. It is fit from the observed SST anomaly field and allows for ENSO nonlinearity, seasonality, and memory effects for prior times. Given that many ENSO behavior features are tightly linked to the nonlinearity in the system (e.g., Choi et al. 2013; DiNezio and Deser 2014; Levine and Jin 2016; Chen et al. 2016), a nonlinear model setting is necessary. The real climate is subjected to a changing forcing, so the detrended data are used to fit the model in order to produce a stationary simulation. Detailed settings are given in the appendix. A 4000-yr stochastic-forced EMR simulation is generated. For simplicity, this simulation is referred to simply as EMR. In later sections, we will show that an EMR fit from the SSTA observation is well behaved and reproduces reasonably realistic ENSO statistics. EMR also has limitations, which will be also discussed.

d. Crude check on GFDL CM2.1 and EMR

Before investigating the detailed ENSO behaviors, we make a crude check of ENSO performance simulated by the EMR and GCM. First we check the main ENSO variability represented in the tropical Pacific SST PC1 (~Niño-3.4). Both the EMR and GCM time series appear reasonably realistic (not shown). Similar to the GFDL CM2.1 run (Wittenberg 2009), the long EMR time series has epochs with energetic ENSO events and epochs with very weak anomalies.

Next we check the ENSO nonlinearity and diversity features represented in the skewed probability density function (PDF) and curved two-dimensional probability density function (2dPDF) of two leading principal components (PC1 and PC2). Kondrashov et al. (2005) and Kravtsov et al. (2005) showed that quadratic nonlinearity is able to overall reproduce the PDF and 2dPDF of a nonlinear system. Chen et al. (2016) further showed that linear models generate an elliptic (symmetric) shape in PC1 and PC2 rather than a curved (asymmetric) shape. We follow the previous studies to coarsely check if these nonlinear features are reproduced. Both EMR and GCM simulations show consistency with OBS in the sign of the skewed distribution of PC1 and PC2, and resemble the curved 2dPDF seen in OBS (Fig. 2). Takahashi et al. (2011) showed that the intermediate coupled ZC model also shows this curved feature in PC1 and PC2.

Note that GFDL CM2.1 has a much stronger nonlinearity represented in a more skewed distribution than OBS. Later analysis using empirical probabilistic diagnostics will show that the strong nonlinearity in GFDL CM2.1 may be one reason for the discrepancy between the model and OBS as to some aspects of ENSO behaviors.

e. CMIP5 models

Assessment of the projected climate change relies heavily on the state-of-the-art coupled general circulation models (e.g., Capotondi et al. 2006; Guilyardi et al. 2003, 2009, 2012; Yu and Kim 2010; Stevenson et al. 2012; Ham and Kug 2012, 2014; Kim and Yu 2012; Bellenger et al. 2014; Taschetto et al. 2014).

In this study, we assess the potential ENSO behavior changes in the twenty-first century using 37 CMIP5

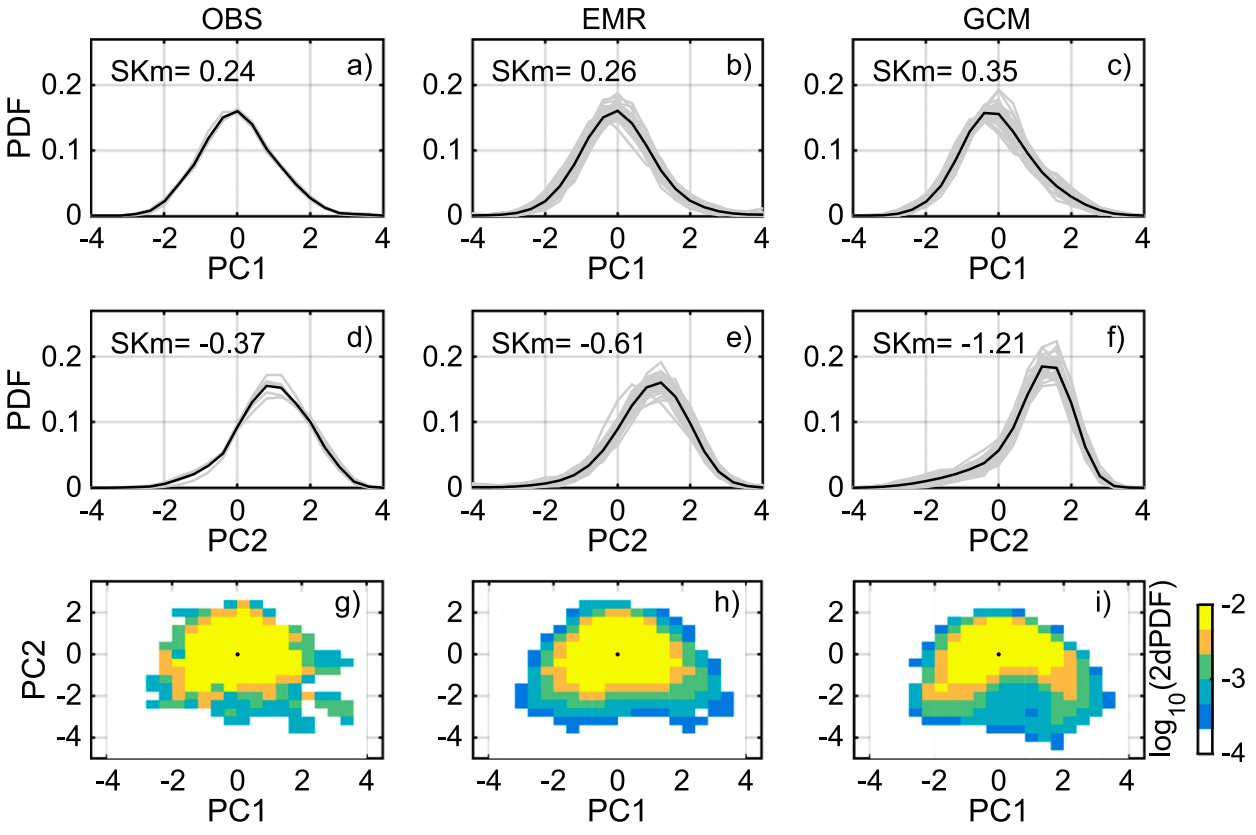

FIG. 2. Simulation evaluation for (left) OBS, (middle) 4000-yr EMR, and (right) 4000-yr GCM, for the (top) probability density function (PDF) of PC1, (d)–(f) PDF of PC2, and (g)–(i) decimal logarithm of the bivariate probability density function (2dPDF) in PC1–PC2 space. In PDF panels, OBS is divided into 5 overlapping 100-yr epochs with 10 years apart. EMR and GCM are both divided into 40 non-overlapping 100-yr epochs. The PDF and the corresponding skewness are calculated in epochs and the average is shown.

models that participated in the Intergovernmental Panel on Climate Change (IPCC) Fifth Assessment Report (AR5) (Table 1). Model descriptions and experiment designs are given in Taylor et al. (2012). We analyzed three sets of simulation experiments: 1) a preindustrial control simulation (PI); 2) the historical simulations, which are integrations from around 1850 to at least 2005 using realistic natural and anthropogenic forcing; and 3) representative concentrating pathway 8.5 (RCP8.5) simulations from the end of the historical runs to 2100 when the radiative forcing reaches 8.5 W m^{-2}. We concatenate on the historical runs (1900–2005) and the RCP8.5 runs (2006–99) and then divide them into the twentieth-century runs (1900–99, denoted as 20C) and the twenty-first-century runs (2000–99; 21C). In the 21C runs, 2000–05 are from the historical run and the remaining years are from the RCP8.5 run. All the PI runs are longer than 200 years. The lengths of the simulations vary for individual models (listed in Table 1). For the PI, 20C, and 21C runs, monthly anomalies are calculated by linearly detrending and subtracting the monthly climatology for the whole period of each run.

3. Method: Empirical probabilistic diagnostics

The diagnostics are carried out in four steps. We first define the ENSO states. We then calculate the occurrence probability of ENSO states for each calendar month, and the transition probability between each ENSO state. After that, we derive a set of probability-based indices for ENSO seasonality (I_{season}), diversity ($I_{cp/ep}$, $I_{e/w}$) and EN–LN asymmetry (I_{amp}, I_{dur}, I_{tra}). These indices are further used to estimate the variation or change of ENSO behaviors.

a. Definition of ENSO states

We define a set of mutually exclusive ENSO states, so that we can categorize each monthly time step into one state and calculate the state transition probabilities. The states are determined using the full length of data in order to investigate ENSO behavior in shorter epochs without changing the definitions of states.

We start from the usual three states: El Niño (EN), neutral (NEU), and La Niña (LN). The normalized tropical Pacific leading PC (PC1) is almost identical to Niño-3.4

TABLE 1. List of 37 CMIP5 models analyzed in this study. Because of the lack of availability in certain models for temperature of ocean surface "tos" we instead analyzed monthly surface temperature "ts" in each model's r1i1p1 run. The first column is the official model name. The second column is the length of preindustrial control run (year). The third to 15th columns are the model rank as shown in each individual figure and panel (e.g., f9b indicates Fig. 9b). The correlating ENSO aspect is labeled in the second row. Note that for individual ENSO behavior models with an asterisk (*) are the 10 models with the smallest error between each model's twentieth-century run (orange ○ in figure) and the twentieth-century observation value (black line in the panel). The last column is the total number of asterisks for each model. The best 10 models, with 5 or more asterisks, are indicated with a plus sign (+) at the end of the model name in the first column. Note that these relative better models are only restricted to ENSO behavior aspects analyzed in this study; this designation is not generally applicable to model performances with regard to other phenomena. For further model center information and experiment designs, see Taylor et al. (2012) and the CMIP5 website (http://cmip-pcmdi.llnl.gov/cmip5/).

Model name	PI	f9b cli	f10b seacli	f9d s.d.	f12a s.k.	f10d $I_{\text{sea-EN}}$	f10f $I_{\text{sea-LN}}$	f11aI $I_{\text{cp/ep-EN}}$	f11c $I_{\text{cp/ep-LN}}$	f11b $I_{e/w\text{-EN}}$	f11d $I_{e/w\text{-LN}}$	f12b I_{amp}	f12c I_{dur}	f12d I_{tra}	num
ACCESS1.0+	250	23*	24*	8	13	5	3	4*	7	17	22*	12	33	11*	5
ACCESS1.3+	500	26*	8	10	22	34	35	13*	6	6*	13	26*	12	7*	5
BCC-CSM1.1	500	22*	5	12	14	2	2	20	3	19	21*	13	13	3*	3
BCC-CSM1.1(m)	400	29*	9	32	29*	9*	5	18	24	29	6	23	3*	27	4
BNU-ESM+	559	25*	11	36	9	11*	18*	5*	30*	35	32	14	5*	25	6
CanESM2	996	17	26*	28	17	14*	17*	19	5	5*	7	19	29	31	4
CCSM4	501	27*	23*	31	34	23	19*	26	37	27	1	35*	11	35	4
CESM1(BGC)	500	28*	14	24	20	29	26	6*	34*	23	11	24	22	30	3
CESM1(CAM5)	319	12	37	29	35	15*	7	36	27*	20	10	31*	17	34	3
CMCC-CESM	277	24*	22*	35	33	33	34	16	23	3	8	32*	21	23	3
CMCC-CM	330	32	27*	9	28*	24	23	8*	25	30	35	28*	19	24	4
CMCC-CMS+	500	30*	29*	23*	16	28	27	14	31*	11*	15*	16	15	17	6
CNRM-CM5	850	19	28*	27	26*	1	1	22	15	34	30	25	18	26	2
CSIRO-Mk3.6.0	500	1	32	22*	4	31	36	34	1	7*	19*	2	31	14	3
FGOALS-g2	700	21	16	18*	7	8	9	12*	13	33	27	7	27	9*	3
FIO-ESM	800	34	6	33	3	18*	14*	3	18	37	31	3	36	2	2
GFDL-CM3	500	10	4	30	12	19	25	28	11	14	4	8	25	29	0
GFDL-ESM2G+	500	5	30*	14*	23*	32	10*	35	26*	4*	5	15	34	13	6
GFDL-ESM2M	500	15	13	37	36	37	32	30	35*	36	20*	36	4*	37	3
GISS-E2-H	240	33	7	3	8	10*	12*	23	2	16	29	11	23	22	2
GISS-E2-H-CC	251	35	12	16*	2	3	13*	27	19	25	14	1	37	20	2
GISS-E2-R	300	36	21*	7	18	6	6	2	22	28	33	21	6*	10*	3
GISS-E2-R-CC	251	37	20	4	1	4	11*	7*	16	31	36	4	24	18	2
HadGEM2-CC	240	8	17	19*	5	20	20	15	14	26	28	6	20	32	1
HadGEM2-ES+	239	9	18	17*	6	12*	8	29	29*	22	17*	5	26	4*	5
INM-CM4	500	13	3	6	24*	27	29	21	4	18	25	20	16	21	1
IPSL-CM5A-LR	1000	7	19	15*	15	30	30	17	21	2	12	18	1*	6*	3
IPSL-CM5A-MR	300	16	10	20*	25*	21	31	25	10	1	9	30*	2*	15	4
IPSL-CM5B-LR+	300	31*	2	11	21	16*	28	1	28*	13*	23*	29*	9*	1	7
MIROC-ESM	531	2	36	1	32*	35	24	32	9	21	37	34*	32	12*	3
MIROC-ESM-CHEM	255	3	35	2	30*	25	21	24	17	15	34	33*	14	5*	3
MIROC5	200	11	31	34	37	22	16*	37	36	32	16*	37	35	36	2
MPI-ESM-LR+	1000	4	34	21*	31*	26	33	11*	20	8*	18*	27*	28	28	6
MPI-ESM-MR	1000	6	33	13	19	36	37	33	12	24	26	17	10*	16	1
MRI-CGCM3+	500	20	1	5	10	17*	22	10*	8	9*	24*	9	7*	8*	6
NorESM1-M+	501	18	15	25	11	13*	15*	9*	33*	12*	3	10	8*	33	6
NorESM1-ME	252	14	25*	26	27*	7	4	31	32*	10*	2	22	30	19	4

with correlation $r = 0.97$, so we define the three-state category as follows: EN is PC1 > 0.7s.d. (PC1), where s.d. denotes one standard deviation. This threshold is generally consistent with the Niño-3.4 > 0.5°C criterion used by the NOAA Climate Prediction Center. Similarly, La Niña is PC1 < −0.7s.d. (PC1); the remainder are defined as NEU.

When ENSO flavors are considered, the three-state category is expanded to five states. For consistency with the three-state category, we use the same PC1 threshold for El Niño/neutral/La Niña. Since EOF2 is a zonal dipole pattern, we use the positive or negative PC2 as the threshold to divide into EP and CP flavors (see Fig. 3). Note that in PC1 and PC2 space, the upper-right domain is for CP El Niño (CPEN), while the lower-left domain is for CP La Niña (CPLN). In OBS, the normalized PC2 is highly correlated ($r = 0.88$) with the difference between

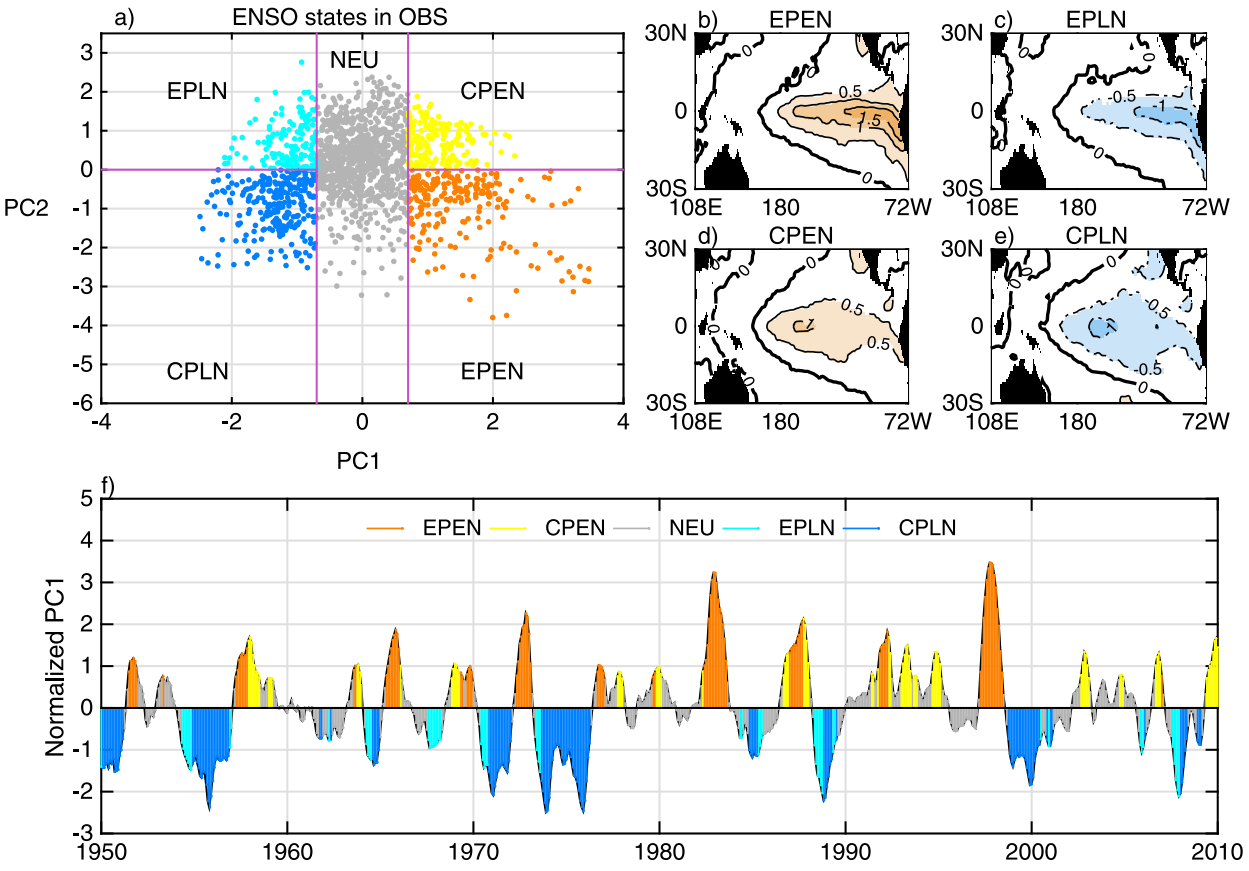

FIG. 3. (a) Definition of five ENSO states (eastern and central Pacific El Niño and La Niña and neutral patterns, denoted EPEN, CPEN, EPLN, CPLN, and NEU) are shown using smoothed monthly PCs from 1870 to the present HadISST v1.1 dataset. The ± 0.7 s.d. (PC1), where s.d. is one standard deviation, is used to distinguish EN/LN from NEU. The zero line of PC2 is used to distinguish EP and CP states. Each state is assigned a color code for further analysis. (b)–(e) The SSTA patterns averaged for eastern/central Pacific ENSO states. (f) Normalized PC1 (1950–2010) with each ENSO state color-coded.

normalized Niño-4 and Niño-3 indices, so the zero PC2 threshold is generally consistent with the EP/CP ENSO categorization using the difference between normalized Niño-4 and Niño-3 indices (e.g., Kug et al. 2009). Typical patterns of the EP/CP flavors of El Niño and La Niña categorized in this diagnostics (Figs. 3b–e) are overall consistent with the patterns defined using Niño indices (Kao and Yu 2009; Kug et al. 2009) or the central Pacific (*C*)/eastern Pacific (*E*) variability indices (*C*/*E* indices) (Takahashi et al. 2011). Table 1 of Yu et al. (2012) listed the major El Niño events from 1950 to 2010 with classification of EP/CP flavor based on three methods. Figure 3f in this study shows a time series of the normalized PC1 from 1950 to 2010, with each ENSO state color-coded to individual month. The comparison indicates that our definition agrees well with the previous studies.

b. Seasonal occurrence probabilities

Based on the above state definitions, the annual mean occurrence probability of each ENSO state is calculated, which gives a climatology probability distribution D_{cli}. For the three-state definition, $D_{cli3} = (P_{EN}, P_{NEU}, P_{LN})$, where $P_{EN} + P_{NEU} + P_{LN} = 1$. Similarly for the five-state definition, $D_{cli5} = (P_{EPEN}, P_{CPEN}, P_{NEU}, P_{EPLN}, P_{CPLN})$, where $P_{EPEN} + P_{CPEN} + P_{NEU} + P_{EPLN} + P_{CPLN} = 1$.

We then measure the occurrence probability of ENSO state in each calendar month, which depicts the seasonal phase-locking features. Full year data are used and thus the sample size for each calendar month is equal. Only the five-state result is shown in Fig. 4; three-state results could be obtained given that $P_{EN} = P_{EPEN} + P_{CPEN}$ and $P_{LN} = P_{EPLN} + P_{CPLN}$. In OBS (Fig. 4a), El Niños and La Niñas both have higher occurrence probabilities of peaking in winter, which agrees with the observed winter phase locking diagnosed in much prior work (e.g., Tziperman et al. 1995, 1997, 1998). In winter El Niños prefer to peak at the eastern Pacific while La Niñas prefer the central Pacific, in agreement with earlier studies on the EN–LN asymmetry (Kang and Kug 2002; Schopf and Burgman 2006; Frauen and Dommenget

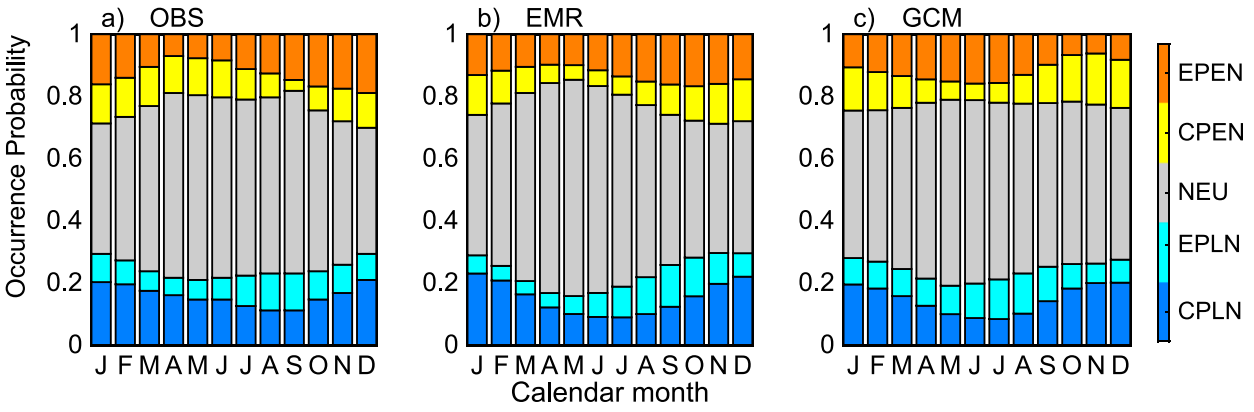

FIG. 4. Monthly occurrence probabilities for five ENSO state in (a) OBS, (b) EMR, and (c) GFDL CM2.1 are shown. Stacked bars along the vertical coordinate are the occurrence probabilities of each color-coded state. The horizontal coordinate is the calendar month from January to December. Full-year data are used so the sample size for each calendar month is equal. In (a), a higher probability of EN/LN in winter months than summer months indicates observed ENSO's winter phase locking. Higher probability of EPEN over CPEN indicates El Niño favors peaking in EP, and higher probability of CPLN over EPLN indicates LN favors peaking in CP.

2010; Dommenget et al. 2013). Turning now to the two simulations, EMR generally reproduces the observed winter phase locking for El Niños (P_{EN}) and La Niñas (P_{LN}), although Fig. 4b shows the CPEN seasonality is a couple of months off from OBS. In GCM (Fig. 4c), La Niñas prefer winter, which agrees with OBS. But El Niños appear to have no seasonal preference (see $P_{\mathrm{EPEN}} + P_{\mathrm{CPEN}}$), which is largely due to the CPENs preferring to peak in winter while EPENs rather favoring summer.

c. *State transition probabilities*

We calculate the transition probability between each ENSO state by tracking their precursors and successors. For example, given k El Niños, among the precursors τ months before there are m_1 El Niños, m_2 La Niñas, and m_3 neutral states ($m_1 + m_2 + m_3 = k$). Among successors τ months later, there are n_1 El Niños, n_2 La Niñas, and n_3 neutral states ($n_1 + n_2 + n_3 = k$). The transition probability from La Niña to El Niño at a τ-month interval is calculated as the conditional probability $P_{\mathrm{LN}(t-\tau)|\mathrm{EN}(t)} = m_2/k$, where t is the time. The transition probability from El Niño to La Niña at a τ-month interval is calculated as $P_{\mathrm{LN}(t+\tau)|\mathrm{EN}(t)} = n_2/k$. The self-transition probability of El Niño across a τ-month interval is calculated as $P_{\mathrm{EN}(t+\tau)|\mathrm{EN}(t)} = n_1/k$ or $P_{\mathrm{EN}(t-\tau)|\mathrm{EN}(t)} = m_1/k$, which are equal by default.

The three-state transition probabilities are shown in Fig. 5. Figure 5a shows the transition of El Niño in OBS. On the positive lead, EN persists [$P_{\mathrm{EN}(t+\tau)|\mathrm{EN}(t)}$] for several months and gradually migrates to La Niña [$P_{\mathrm{LN}(t+\tau)|\mathrm{EN}(t)}$] or neutral [$P_{\mathrm{NEU}(t+\tau)|\mathrm{EN}(t)}$] in about one year. At about three years or even longer intervals as $\tau \to \infty$, the transition converges toward the climatology distribution. In OBS, the asymmetry in transition between El Niño and La Niña is not substantial. In EMR, the transition characteristics agree with OBS. In GCM, the EN–LN transition asymmetry is much greater than OBS with a large discrepancy between $P_{\mathrm{LN}(t-\tau)|\mathrm{EN}(t)}$ and $P_{\mathrm{LN}(t+\tau)|\mathrm{EN}(t)}$ at $\tau \sim$ 1 to 2 years.

Similarly we calculate the five-state transition probabilities. Here we mainly focus on the favored zonal propagation direction of El Niño and La Niña (Fig. 6). In OBS, the fact that $P_{\mathrm{EPEN}(t-\tau)|\mathrm{CPEN}(t)} > P_{\mathrm{EPEN}(t+\tau)|\mathrm{CPEN}(t)}$ across 0–6 months (Fig. 6a) indicates that El Niños favor westward propagation from EP El Niño (EPEN) to CPEN. Similarly, $P_{\mathrm{CPLN}(t-\tau)|\mathrm{EPLN}(t)} < P_{\mathrm{CPLN}(t+\tau)|\mathrm{EPLN}(t)}$ across 0–6 months (Fig. 6b) indicates that La Niñas also favor westward propagation from EP La Niña (EPLN) to CPLN. In EMR, the zonal transition of both El Niños and La Niñas agree with OBS (Figs. 6c,d). In GCM, La Niñas favor westward propagation, similar to OBS (Fig. 6f). But El Niños differ from OBS by favoring eastward propagation (Fig. 6e).

Probability measures show that individual ENSO behaviors have varying representative time scales. So we later define the indices based on the transition probabilities at their respective time scales. In the three-state transition, we mainly focus on the persistence (self transition) of El Niño and La Niña within 0–36 months and asymmetry in the EN–LN transition across 0–18 months. In the five-state transition, we mainly focus on the zonal propagation of El Niño (asymmetry in the EPEN–CPEN transition) and the zonal propagation of La Niña (asymmetry in the EPLN–CPLN transition) across 0–6 months. Other transition probability results [e.g., transition to/from NEU, self-transition of EP/CP ENSO states, and EN–LN transitions specifying EP/CP

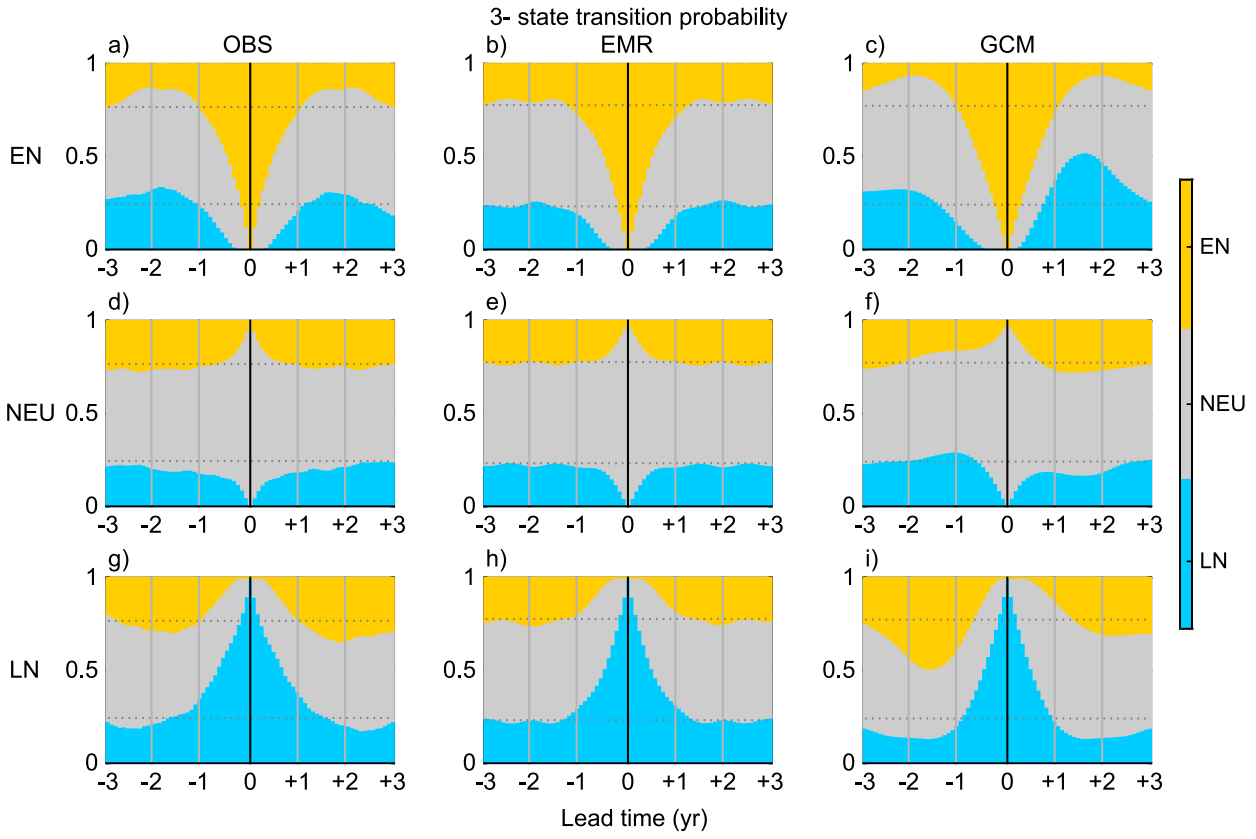

FIG. 5. State transition probabilities for (a)–(c) EN, (d)–(f) NEU, and (g)–(i) LN in (left) OBS, (middle) EMR, and (right) GFDL CM2.1 GCM. The horizontal coordinate represents the transition from the past (−3 yr) to the future (+3 yr) in monthly intervals, with zero indicating the current state. Taking GCM EN transition [in (c)] for example, bars along the vertical coordinate at +1 yr (+12 months) represent the self-transition probability $P_{\mathrm{EN}(t+\tau)|\mathrm{EN}(t)}$ (upper bar), the $P_{\mathrm{NEU}(t+\tau)|\mathrm{EN}(t)}$ (middle bar) and the opposite-sign transition $P_{\mathrm{LN}(t+\tau)|\mathrm{EN}(t)}$ (lower bar). The decaying of $P_{\mathrm{EN}(t+\tau)|\mathrm{EN}(t)}$ as function of lead time indicates EN's duration. The discrepancy between $P_{\mathrm{LN}(t-\tau)|\mathrm{EN}(t)}$ (lead < 0 side) and $P_{\mathrm{LN}(t+\tau)|\mathrm{EN}(t)}$ (lead > 0 side) indicates the EN–LN asymmetry in transition. The transition probabilities generally converge to the climatology, i.e., the nonseasonal occurrence probability of each state (dotted line in each panel).

information such as $P_{\mathrm{EPEN}(t-\tau)|\mathrm{CPLN}(t)}$] are not included in the following set of ENSO behavior indices but are left for future study.

Here we use both forward and reverse conditional probability to characterize the transition, which is based on the following consideration. In a stationary process, transition probability across a long time interval converges to the climatology. Note that $\lim_{\tau\to\infty} P_{\mathrm{LN}(t+\tau)|\mathrm{EN}(t)} = P_{\mathrm{LN}}$, while $\lim_{\tau\to\infty} P_{\mathrm{EN}(t+\tau)|\mathrm{LN}(t)} = P_{\mathrm{EN}}$. To characterize the transition asymmetry, these two conditional probabilities need to be both normalized by their according occurrence probability or one needs to be rescaled to match the other one. Here we use El Niño as the base state, and the asymmetry is then calculated using the discrepancy $dP_{\mathrm{EN-LN}} = P_{\mathrm{LN}(t+\tau)|\mathrm{EN}(t)} - P_{\mathrm{EN}(t+\tau)|\mathrm{LN}(t)}/P_{\mathrm{EN}} \times P_{\mathrm{LN}}$. Given Bayes' rule, we obtain $dP_{\mathrm{EN-LN}} = P_{\mathrm{LN}(t+\tau)|\mathrm{EN}(t)} - [P_{\mathrm{LN}(t)|\mathrm{EN}(t+\tau)} \times P_{\mathrm{EN}}/P_{\mathrm{LN}}]/P_{\mathrm{EN}} \times P_{\mathrm{LN}} = P_{\mathrm{LN}(t+\tau)|\mathrm{EN}(t)} - P_{\mathrm{LN}(t-\tau)|\mathrm{EN}(t)}$. So both the forward conditional probability $P_{\mathrm{LN}(t+\tau)|\mathrm{EN}(t)}$ and the reverse conditional probability $P_{\mathrm{LN}(t-\tau)|\mathrm{EN}(t)}$ are shown in Fig. 5 to illustrate the transition asymmetry. If we use La Niña as the base state instead, $dP_{\mathrm{EN-LN}} = [P_{\mathrm{EN}(t-\tau)|\mathrm{LN}(t)} - P_{\mathrm{EN}(t+\tau)|\mathrm{LN}(t)}]/P_{\mathrm{EN}} \times P_{\mathrm{LN}}$ gives the same result. Similarly, we characterize the zonal transition of El Niño based on CPEN and the discrepancy $dP_{\mathrm{CPEN-EPEN}} = [P_{\mathrm{EPEN}(t+\tau)|\mathrm{CPEN}(t)} - P_{\mathrm{EPEN}(t-\tau)|\mathrm{CPEN}(t)}]$. It could be also calculated based on EPEN: $dP_{\mathrm{CPEN-EPEN}} = [P_{\mathrm{CPEN}(t-\tau)|\mathrm{EPEN}(t)} - P_{\mathrm{CPEN}(t+\tau)|\mathrm{EPEN}(t)}]/P_{\mathrm{CPEN}} \times P_{\mathrm{EPEN}}$. For the zonal transition of La Niña, we calculate the discrepancy $dP_{\mathrm{CPLN-EPLN}} = P_{\mathrm{CPLN}(t-\tau)|\mathrm{EPLN}(t)} - P_{\mathrm{CPLN}(t+\tau)|\mathrm{EPLN}(t)}$ based on EPLN. If based on CPLN instead, then $dP_{\mathrm{CPLN-EPLN}} = [P_{\mathrm{EPLN}(t+\tau)|\mathrm{CPLN}(t)} - P_{\mathrm{EPLN}(t-\tau)|\mathrm{CPLN}(t)}]/P_{\mathrm{EPLN}} \times P_{\mathrm{CPLN}}$ gives the same result.

d. A set of indices for ENSO behaviors

Here we define a set of indices to measure various aspects of ENSO behavior in a period of 100 years. OBS is divided into five 100-yr overlapping epochs starting

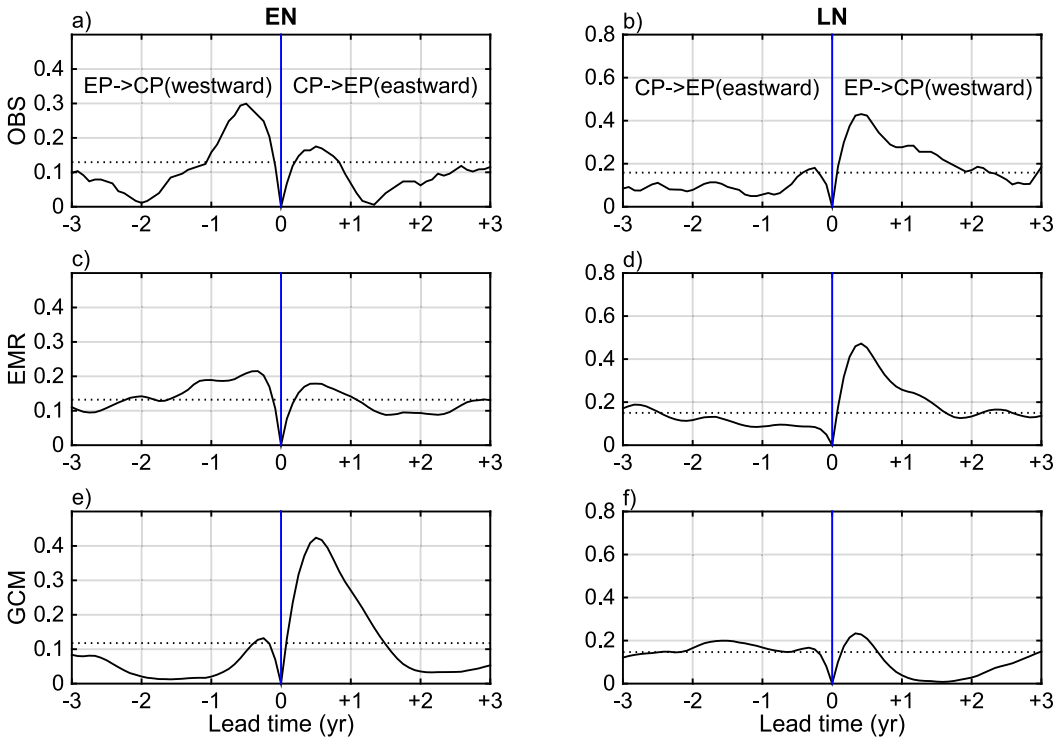

FIG. 6. Zonal propagation asymmetry in (a),(b) OBS, (c),(d) EMR, and (e),(f) GCM. (left) Transition probabilities conditioned on CPEN state $P_{\mathrm{EPEN}(t-\tau)|\mathrm{CPEN}(t)}$ (negative lead) and $P_{\mathrm{EPEN}(t+\tau)|\mathrm{CPEN}(t)}$ (positive lead), which generally converge to the occurrence probability P_{EPEN} (dotted line) toward a large lead time. (right) Transition probabilities conditioned on EPLN state $P_{\mathrm{CPLN}(t-\tau)|\mathrm{EPLN}(t)}$ (negative lead) and $P_{\mathrm{CPLN}(t+\tau)|\mathrm{EPLN}(t)}$ (positive lead), which generally converge to the occurrence probability P_{CPLN} (dotted line).

10 years apart. The 4000-yr simulations of EMR and GCM are divided into 391 overlapping 100-yr epochs also starting 10 years apart. We first summarize the ENSO behaviors in OBS and then discuss EMR and GCM.

A seasonality index I_{sea} is defined to identify the favored peak season for a given epoch. For El Niños, I_{sea} is the total occurrence of El Niño in the summer half year (March–August) divided by the total occurrence of El Niño in the winter half year (September–February). $I_{\mathrm{sea}} < 1$ (>1) indicates El Niño preferentially peaks in winter (summer). The results (Figs. 7a,d) show that both El Niños and La Niñas in OBS prefer winter. In EMR, El Niños and La Niñas also prefer the winter half year in all epochs. In GCM, La Niñas mainly prefer winter, consistent with OBS and EMR, but for El Niños, I_{sea} is more centered around a value of 1, suggesting that the majority of epochs do not have notable seasonal preferences. This agrees with the seasonal occurrence probability results in Fig. 4.

A diversity index $I_{\mathrm{cp/ep}}$ is defined for El Niños to diagnose the dominant peak location in a given epoch, calculated as the total occurrence of CPEN divided by the total occurrence of EPEN. If $I_{\mathrm{cp/ep}} < 1$ (>1), this indicates that El Niño prefers to peak at EP (CP). There is a similar definition for La Niña. The results (Figs. 7b,e) show that EPENs and CPLNs dominate in OBS. In EMR, 91% of epochs are dominated by EPEN and 97% of epochs are dominated by CPLN. The GCM overall agrees with the OBS and EMR, with most epochs favoring EPENs and CPLNs.

Another diversity index $I_{e/w}$ is defined to diagnose the dominant zonal propagation in a given epoch. For El Niños, $I_{e/w}$ is the average of $dP_{\mathrm{CPEN-EPEN}}$ within a 6-month interval. For La Niñas, $I_{e/w}$ is the average of $dP_{\mathrm{CPLN-EPLN}}$ within a 6-month interval. If $I_{e/w} < 0$ (>0), this indicates preferring westward (eastward) propagation. Figures 7c and 7f show that OBS has more westward moving El Niños and La Niñas. In EMR, El Niños favor westward propagation in 74% of epochs while La Niñas favor westward propagation in all epochs. In GCM, more than half the epochs favor westward propagating La Niñas, which is generally consistent with OBS and EMR. But all epochs favor eastward propagating El Niños, which is not realistic. This model discrepancy agrees with the five-state transition results (Fig. 6).

The asymmetry index I_{amp}, which diagnoses the relative amplitude of El Niño and La Niña in a given epoch,

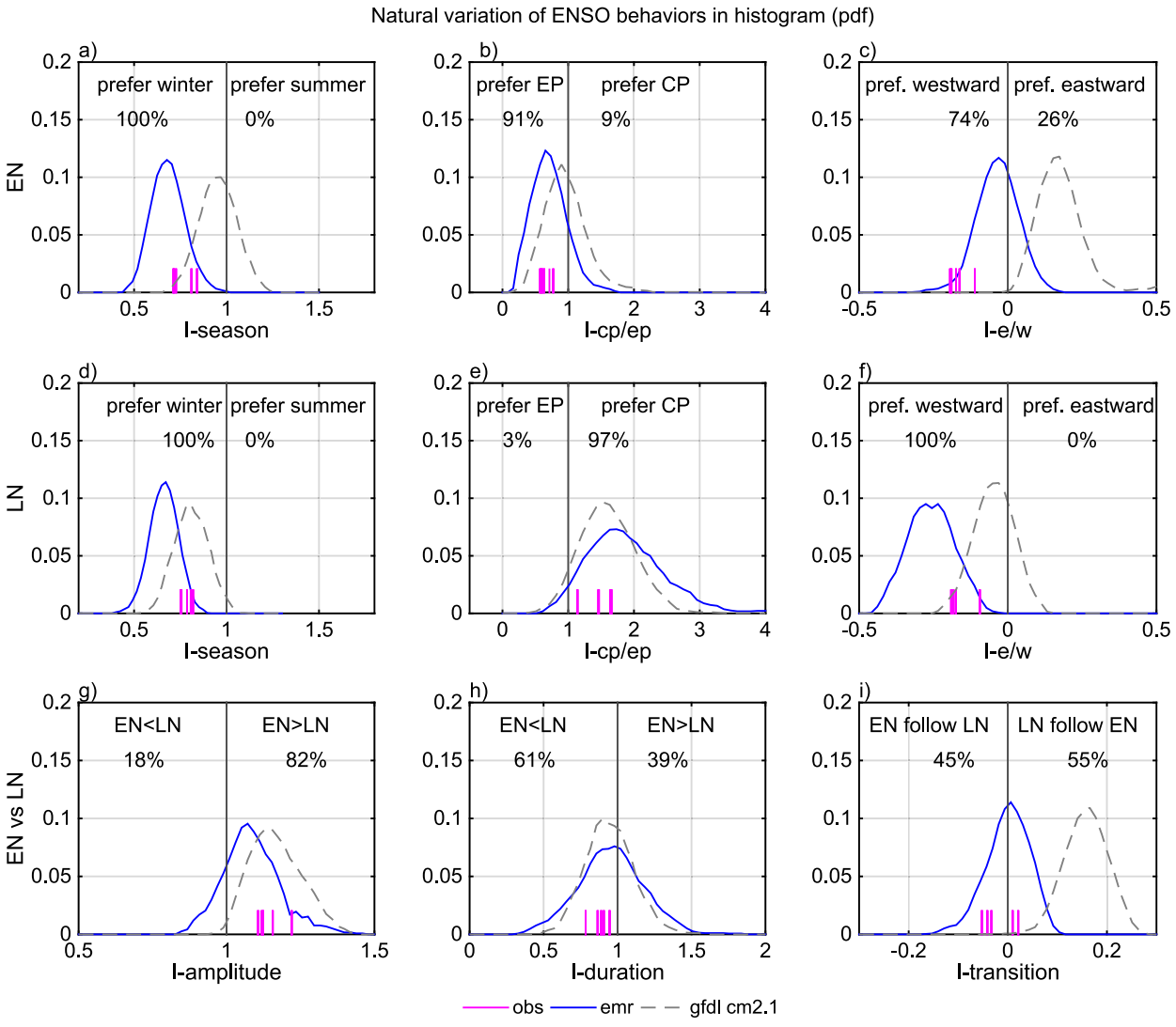

FIG. 7. Variation of ENSO behaviors in 4000-yr EMR and GFDL CM2.1 GCM simulation. Each index (see text for definitions) is calculated in 100-yr overlapping epochs 10 years apart. The PDF is shown in the blue curve or the dashed curve. Index values in epochs of OBS are shown in magenta lines (five in total). (top) ENSO diversity indices, including I_{sea}, $I_{cp/ep}$, and $I_{e/w}$, are shown for El Niño and La Niña. (bottom) EN–LN asymmetry indices, including I_{amp}, I_{dur}, and I_{tra}. For each panel, the percentage of epochs in the EMR satisfying the specified index range is shown. Taking (b) for example, OBS have more EPEN than CPEN ($I_{cp/ep} < 1$). Among the 391 century-long epochs in EMR, 91% of epochs have more EPEN than CPEN.

is calculated as the mean of PC1 value for El Niño months in 100 years divided by the mean of PC1 value for La Niña months. If $I_{amp} > 1$, this indicates that the overall amplitude of El Niño is larger than La Niña. Figure 7g shows that El Niños have larger amplitude than La Niñas in OBS. In EMR, 82% of epochs have $I_{amp} > 1$. GCM generally agrees with OBS and EMR.

Another asymmetry index I_{dur} diagnoses the relative duration of El Niño and La Niña in a given epoch. It is calculated as the mean of El Niño self-transition probabilities $P_{EN(t+\tau)|EN(t)}$ within a 36-month interval divided by the mean of La Niña self-transition probabilities $P_{LN(t+\tau)|LN(t)}$ within a 36-month interval. If $I_{dur} < 1$, this indicates that La Niña is more durable. Figure 7h shows that La Niña is more durable in OBS. In EMR 61% of epochs have more durable La Niñas. GCM agrees well with EMR and OBS.

A third asymmetry index I_{tra}, which diagnoses the transition asymmetry between El Niño and La Niña, is calculated as average of dP_{EN-LN} within an 18-month interval. If $I_{tra} > 0$, this indicates that La Niñas tightly follow El Niños more than vice versa. Figure 7i shows that in OBS the asymmetry in transition is not substantial. For the twentieth-century epoch, it has a slightly positive

asymmetry with $I_{tra} > 0$ (shown in Fig. 12d along with CMIP5 models). In EMR, 55% of epochs have $I_{tra} > 0$. Compared to OBS and EMR, GCM shows a much larger asymmetry in transition, with all epochs favoring La Niña tightly following El Niño. This discrepancy agrees with the three-state transition in Fig. 5. Our results is generally consistent with Choi et al. (2013), in which the EN–LN transition is defined based on individual events with the time range set to 12 months.

4. Natural variation of ENSO behaviors

In this section, we first summarize the performance of ENSO behaviors in two simulations. GFDL CM2.1 serves as one example for the fully coupled GCMs and EMR is one example for the data-driven models. We then discuss how the simulated ENSO behaviors depend on the model nonlinearity. We last present an overview of the natural variation of the ENSO behaviors.

a. GFDL CM2.1

Figures 4–7 show that GFDL CM2.1 overall agrees with OBS and EMR as to some aspects of the ENSO behavior, such as the ratio of CP to EP ENSO (Figs. 7b,e), El Niño–La Niña asymmetry in amplitude (Fig. 7g), and duration (Fig. 7h). It is mainly biased from OBS in three aspects, including the seasonality (Figs. 4 and 7a,d), EN–LN transition (Figs. 5 and 7i), and the zonal propagation (Figs. 6 and 7c,f).

We then briefly discuss these three biases. As to the seasonal phase locking, El Niños in GFDL CM2.1 do not show a notable seasonal preference (Fig. 4), which is mainly due to the competing impacts of EPEN peaking in summer and CPEN peaking in winter. Overall, SST anomaly peaks when the collective positive feedbacks are balanced by the negative feedbacks (e.g., Tziperman et al. 1995, 1997, 1998; Neelin et al. 2000; An and Wang 2001; Xiao and Mechoso 2009; Stein et al. 2010). In GFDL CM2.1, the biases in positive and negative feedbacks may together alter the SSTA peak timing and location. Wittenberg et al. (2006) once showed that GFDL CM2.1 simulated events tend to peak either in summer or in winter. This bias is likely tied to the semiannual cycle of the background convection and currents, which is associated with a double ITCZ and the seasonal reversal of the meridional SST gradient and winds in the eastern Pacific.

As to the EN–LN transition and the zonal propagation, all epochs of GFDL CM2.1 show a strong transition asymmetry with La Niñas tightly following El Niños (Fig. 7i) and all epochs favor eastward propagating El Niños (Fig. 7c). GFDL CM2.1 is largely biased so that its variation range does not even cover the observations. If only century-long rather than 4000-yr GFDL CM2.1 simulations are available, the biases in these two aspects might be the most distinguishable from OBS.

In this study we do not have a special category for the extreme El Niños since only a few extreme El Niños occurred in OBS. The overall ENSO statistics in the observations are dominated by the moderate events. GFDL CM2.1 has overly strong El Niño with many extreme events (Wittenberg 2009; Takahashi and Dewitte 2016; Levine and Jin 2016). Extreme El Niños usually peak in the eastern Pacific, whreas moderate El Niños peak either in the central Pacific or in the eastern Pacific (Kug et al. 2009; Takahashi and Dewitte 2016). Extreme El Niños tend to propagate eastward and moderate El Niños propagate westward (Santoso et al. 2013; Kim and Cai 2014). Extreme El Niños are also associated with a large EN–LN asymmetry in transition (Choi et al. 2013). Thus the statistics in GFDL CM2.1 are largely shifted by extreme events to favor more eastward propagating El Niños and much strong asymmetry in EN–LN transition. These behavior biases could be further traced back to the model's overly strong nonlinearity, which is also manifested in, for example, the largely skewed probability density function of SSTA in Fig. 2.

We also notice that GFDL CM2.1 does better with SSTA associated with La Niña than El Niño, especially for seasonality and zonal propagation. Since the coupling only becomes nonlinear above a certain temperature threshold (Takahashi and Dewitte 2016; Levine and Jin 2016), El Niños (as a warming anomaly on top of the mean temperature) are more sensitive to the extent of nonlinearity in the system than La Niñas (a cooling anomaly). This may be one reason why La Niñas do not show as greater a diversity as El Niños in Kug and Ham (2011). A good performance for El Niño demands that the strength of the model's nonlinearity resemble that in the real climate. On the contrary, La Niñas may still be simulated realistically even for a model with a too strong nonlinearity.

b. EMR

Figures 4–7 show that EMR overall agrees with OBS as to most aspects of ENSO behaviors, such as seasonal phase locking (Figs. 4 and 7a,d), the ratio of CP to EP ENSO (Figs. 7b,e), El Niño–La Niña asymmetry in amplitude (Fig. 7g), duration (Fig. 7h), and transition (Figs. 5 and 7i). It shows slight biases for zonal propagation (Figs. 6 and 7c,f).

The EMR is built to capture the transition from one month to the next, which includes some nonlinear dynamics, memory effects from a single prior time step, and annual periodic terms. On the one hand, the results

that EMR overall agrees with OBS as to the nonlinear measure 2dPDF in Fig. 2h and for the seasonal phase locking in Fig. 4 are expected. On the other hand, EMR does not explicitly build in different peak locations, different propagation directions, or the EN–LN asymmetry in amplitude, duration, and transition. Its ability to capture these aspects is an implicit and nonobvious consequence of the model construction. Its extended behaviors in the long runs are at least as plausible as the GCM. Moreover, as a low-order empirical model, an EMR simulation is computationally efficient.

c. *ENSO behavior dependence on nonlinearity*

GFDL CM2.1's biases with regard to ENSO behavior suggest that simulated ENSO behavior is very sensitive to the model nonlinearity, especially the asymmetry between El Niño and La Niña. In this section, we fit a linear EMR model (EMR-L) to the observation (details in the appendix) and generate a 4000-yr simulation. In total we compare the ENSO behaviors in four systems with varying levels of nonlinearity: EMR-L, OBS, EMR, and GFDL CM2.1. The results are shown in Fig. 8.

We first discuss the ENSO behavior simulated in the linear system, and then compare with other systems. In the linear model simulation, 2dPDF in PC1–PC2 space is centered at zero without a curved shape (Fig. 8b), which is as expected. There is also no notable EN–LN asymmetry in amplitude (Fig. 8e), duration (Fig. 8f), and transition (Fig. 8g). Both El Niño and La Niña prefer winter peaking (Fig. 8h). There is no EP/CP preference for peaking location (Fig. 8i). Both El Niño and La Niña favor west propagating (Fig. 8j). The distribution of El Niño and La Niña are almost identical. Overall, ENSO behaviors in the linear system lack of the EN–LN asymmetries, which indicates that the nonlinearity is necessary to create the EN–LN asymmetry.

Using the linear EMR as a reference, we then discuss the ENSO behaviors in the nonlinear EMR. It reproduces the curved 2dPDF in PC1 and PC2. An EN–LN asymmetry appears in amplitude and duration, although it is still not notable for transition. As to the peak season, El Niño and La Niña start to show a small discrepancy (Fig. 8k). As to the peak location, El Niño prefers the eastern Pacific and La Niña prefers the central Pacific (Fig. 8l), and this asymmetry agrees with the observation. As to the zonal propagation, El Niños start to shift a bit toward favoring eastward while La Niñas shifting toward favoring westward (Fig. 8m).

Then we discuss the ENSO behaviors in the strong nonlinear GFDL CM2.1. It reproduces the 2dPDF with a larger curvature. It shows a larger EN–LN asymmetry in amplitude, duration, and transition. As to the peak season, El Niño and La Niña show a larger difference (Fig. 8n). Distribution of El Niño shifts toward favoring summer peaking. As to the peak location, El Niño prefers the eastern Pacific and La Niña prefers the central Pacific (Fig. 8o). As to the zonal propagation, La Niñas still favor westward propagation while El Niños favor eastward propagation.

We previously discussed that GFDL CM2.1 shows a better performance for La Niña compared to El Niño. Here the comparison between linear and nonlinear system also suggests that, when the system become more nonlinear, La Niñas better preserve its usual characteristics, whereas El Niños are very sensitive so the characteristics may change quickly and exhibit a larger diversity.

Model nonlinearity is influenced by many different physical processes. DiNezio and Deser (2014) addressed the nonlinear controls on the persistence of La Niña using a 1300-yr simulation of the CCSM4 model. The authors fit a nonlinear delayed oscillation model that illustrates that the nonlinearity in the delayed thermocline feedback plays a role for the persistence of La Niña. Takahashi and Dewitte (2016) have shown that moderate and strong nonlinear ENSO regimes exist. They found that extreme El Niño events simulated by GFDL CM2.1 have consistent temporal evolutions as the observed strong El Niños. So a GFDL CM2.1 simulation is analyzed to reconstruct a robust evolution profile for SST, wind stress, and the thermocline tilting. The authors also showed that the existence of these regimes is very likely due to the nonlinearity in the Bjerknes feedback.

In summary, comparison of EMR-L, EMR, and GFDL CM2.1 shows that a nonlinear model is necessary to reproduce the comprehensive ENSO behaviors including the EN–LN asymmetry. For a given nonlinear model, it is also important that this model has a proper extent of model nonlinearity that resembles the reality. The results also show that the nonlinearity mainly influences the ENSO behavior by controlling the extent of the EN–LN asymmetry. El Niños are more sensitive to the system nonlinearity and exhibit a larger diversity than the La Niñas.

d. *Overview of ENSO behavior variations*

GFDL CM2.1 may provide a reasonable estimate for variation of EP/CP ENSO flavors, but may not be suitable for the zonal propagation and the EN–LN transition. EMR is overall better for nine aspects. Note that EMR's nonlinearity may be also slightly larger than OBS, which might be further adjusted in the future study. Before a better model becomes available, the current EMR model is still useful to provide a relatively realistic estimate for ENSO behaviors.

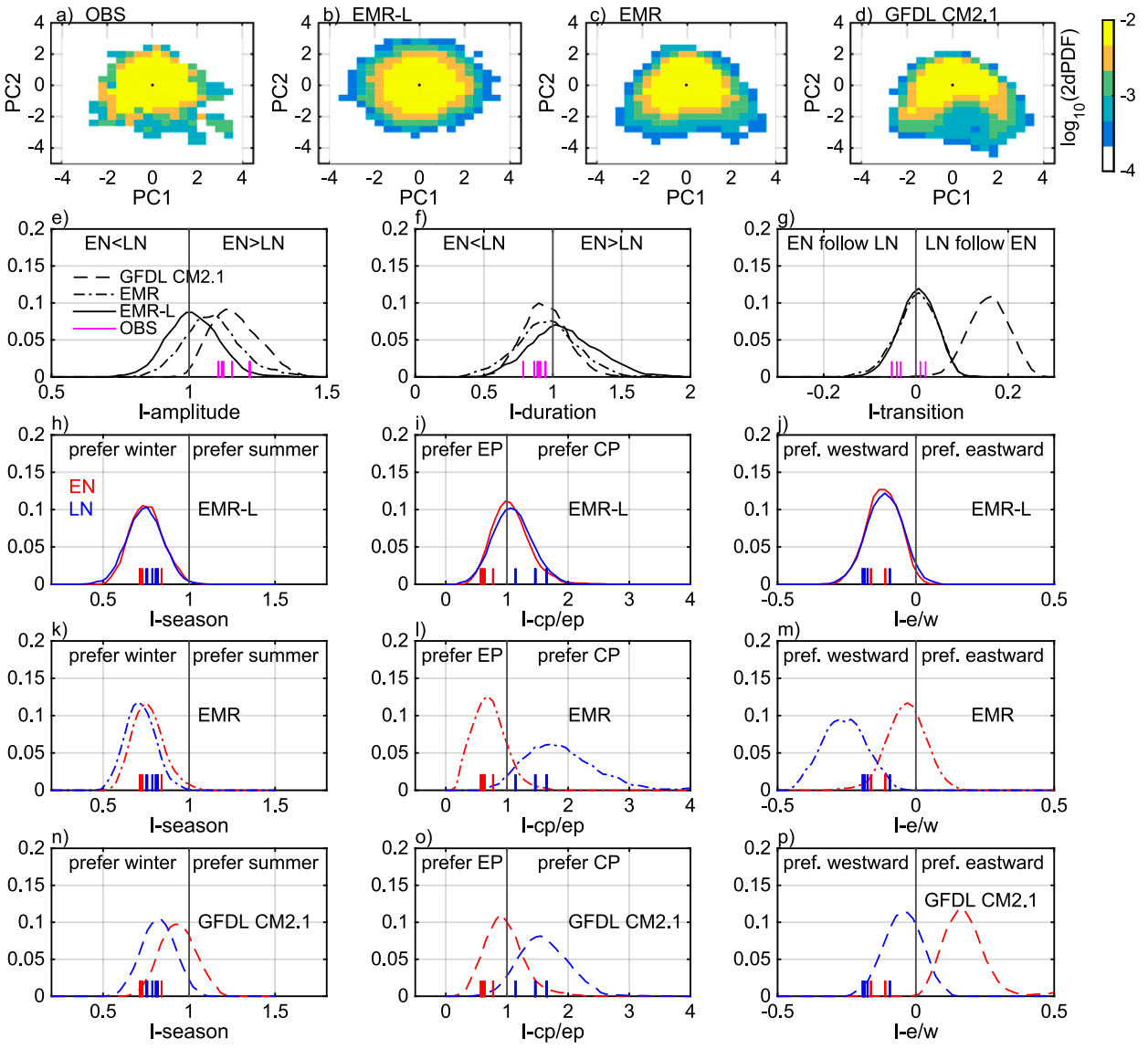

FIG. 8. ENSO behaviors in OBS, a linear EMR (EMR-L), a nonlinear EMR and GFDL CM2.1. (a)–(d) Decimal logarithm of the bivariate probability density function (2dPDF) in PC1–PC2 space. For all other panels the distribution is calculated in 100-yr overlapping epochs 10 years apart. (e)–(g) I_{amp}, I_{dur}, and I_{tra}, for observation (magenta), EMR-L (solid black curve), EMR (dash-dotted curve),and GFDL CM2.1 (dashed curve). Also shown are (h),(k),(n) I_{sea}, (i),(l),(o) $I_{cp/ep}$, and (j),(m),(p) $I_{e/w}$, with El Niño in red and La Niña in blue.

We now summarize the natural variation of ENSO behavior given by EMR. Under the white noise forcing without a trend, epochs with ENSO peaking in summer and epochs favoring eastward propagating La Niñas are still not likely, but the following scenarios may occur with a certain likelihood: epochs with El Niño preferring central Pacific (9%), epochs with La Niña favoring eastern Pacific (3%), epochs preferring eastward propagating El Niños (26%), epochs with La Niña having larger amplitude than El Niño (18%), epochs with more persist El Niño than La Niña (39%), and epochs with a quicker transition from La Niña to El Niño (45%). Under stochastic noise, epochs with characteristics different from the past 100-yr OBS could occur. One needs to be cautious when attributing the unusual ENSO variations for a certain period as a response to the changing external forcing.

e. *Uncertainty in estimates of the true distribution*

We have calculated a distribution of indices from overlapping 100-yr epochs of a long (4000 yr) model simulation. Note that model-reconstructed distribution is not constrained to be centered at the OBS samples. Usually such a match is built in by resampling the data or

sampling from an assumed distribution (e.g., Gaussian) with specified sample mean and standard deviation. Both the GCM and EMR distributions are based on 391 samples while the OBS distribution is based on only five samples. The OBS sample distribution, as an approximation to the unknown true distribution, is used as the metric to examine the modeled distributions. Given only a few available OBS samples, its distribution may not reflect the statistics of the true distribution (Wittenberg 2009). The shortness of the OBS record also makes it difficult to establish that a model distribution is significantly different from OBS.

We apply the Kolmogorov–Smirnov (KS) test to estimate whether or not two distributions are alike. KS tests show that among the nine aspects in Fig. 7, the EMR and GCM distributions are significantly different for eight of them with $p < 10^{-3}$, while for I-dur $p = 0.02$. The GCM distributions of $I_{\mathrm{cp/ep-LN}}$, I_{amp}, I_{dur}, and $I_{\mathrm{season-LN}}$ are not significantly different from OBS distribution while the GCM distributions of $I_{\mathrm{season-EN}}$, $I_{\mathrm{cp/ep-EN}}$, $I_{e/w-\mathrm{EN}}$, $I_{e/w-\mathrm{LN}}$, and I_{tra} differ from OBS at greater than the 1% level ($p < 0.01$). With the same significance level, EMR distribution differs from the OBS distributions for $I_{\mathrm{season-EN}}$, $I_{\mathrm{season-LN}}$, $I_{e/w-\mathrm{EN}}$, and $I_{e/w-\mathrm{LN}}$.

Besides the uncertainty coming from the shortage of data to fit and constrain robust model coefficients for the data-driven models, another aspect of uncertainty comes from the model construction itself. We showed in Chen et al. (2016) that there are many different ways to formulate an EMR or other low-order models. It is difficult to construct one particular model that captures every conceivable feature. Although the current version of EMR including nonlinearity, memory effect, and seasonality is the overall best choice in the study, it fails to match OBS's distribution closely for a few aspects. We use EMR as an example to illustrate both using a data-driven model and a GCM to estimate the natural variation of the ENSO characteristics. Both models are flawed and the bias correction is a potential topic for future study.

5. ENSO behavior change in the twenty-first century

In this section, we analyze whether the ENSO behaviors may exhibit notable changes from the twentieth to the twenty-first century using CMIP5 projections under the RCP8.5 scenario. Besides the aforementioned ENSO behaviors, we also estimate the annual mean SST, annual cycle, standard deviation, and skewness of SSTA in Niño-3.4 region.

When we analyze the CMIP5 models, we notice that the PC-based definition for ENSO diversity works well for the models with correct representations of EOF1 and EOF2, but this definition may not be optimal for the models with poor performance on ENSO diversity. So we will use a similar but Niño-based definition for CMIP5 model evaluation. Normalized Niño-3.4 replaces normalized PC1. Normalized Niño-4 minus normalized Niño-3 replaces normalized PC2. All are normalized to have standard deviation equal to one.

We will first evaluate whether 37 CMIP5 models could reproduce realistic statistics (as compared with the observation in the twentieth century). The results from each model are sorted in an ascending order for individual aspects of ENSO behavior. Table 1 gives the model rank for each aspect. A multimodel mean (MMM) for 37 models is calculated to represent an overall performance of CMIP5 models. After that we compare the number of models projecting an increase or a decrease to assess whether the projected changes for the twenty-first century are supported with sufficient model agreement.

We next identify if an apparent change is a significant response to the changing external forcing. For each individual model, the change from the twentieth to the twenty-first century is viewed as a significant change if satisfying one of the following: 1) $I_{21\mathrm{C}} > I_{20\mathrm{C}}$ (increase) and $I_{21\mathrm{C}} >$ 97.5th percentile of PI run or 2) $I_{21\mathrm{C}} < I_{20\mathrm{C}}$ (decrease) and $I_{21\mathrm{C}} <$ 2.5th percentile of PI run, where $I_{20\mathrm{C}}(I_{21\mathrm{C}})$ is the given index calculated for the twentieth (twenty-first) century.

Note that there is a large spread of the natural variation given by each model's PI runs, so an additional estimate of the natural variation is provided as reference using the aforementioned 4000-yr stochastic-forced EMR simulation fit from OBS.

a. SST climatology and anomaly

We first investigate whether these CMIP5 models reproduce a realistic tropical Pacific climatology. The time series of Niño-3.4 SST from 1900 to 2100 are shown in Fig. 9a. Niño-3.4 SST averaged in the twentieth century (20C) and twenty-first century (21C) are shown in Fig. 9b. The averaged Niño-3.4 SST in sliding 100-yr epochs for the preindustrial control run (PI) is also provided as reference. There is a considerable spread compared to observations in 20C runs, and the MMM of 37 models slightly underestimates the 20C mean SST. All 37 models project a warming future for the RCP8.5 scenario with an ~2°C temperature increase. The changes are significant in all models.

The Niño-3.4 SST anomalies in 20C and 21C are obtained by linearly detrending and removing monthly climatology in each 100-yr segment (Fig. 9c) and the standard deviation (s.d.) of Niño-3.4 is shown in Fig. 9d.

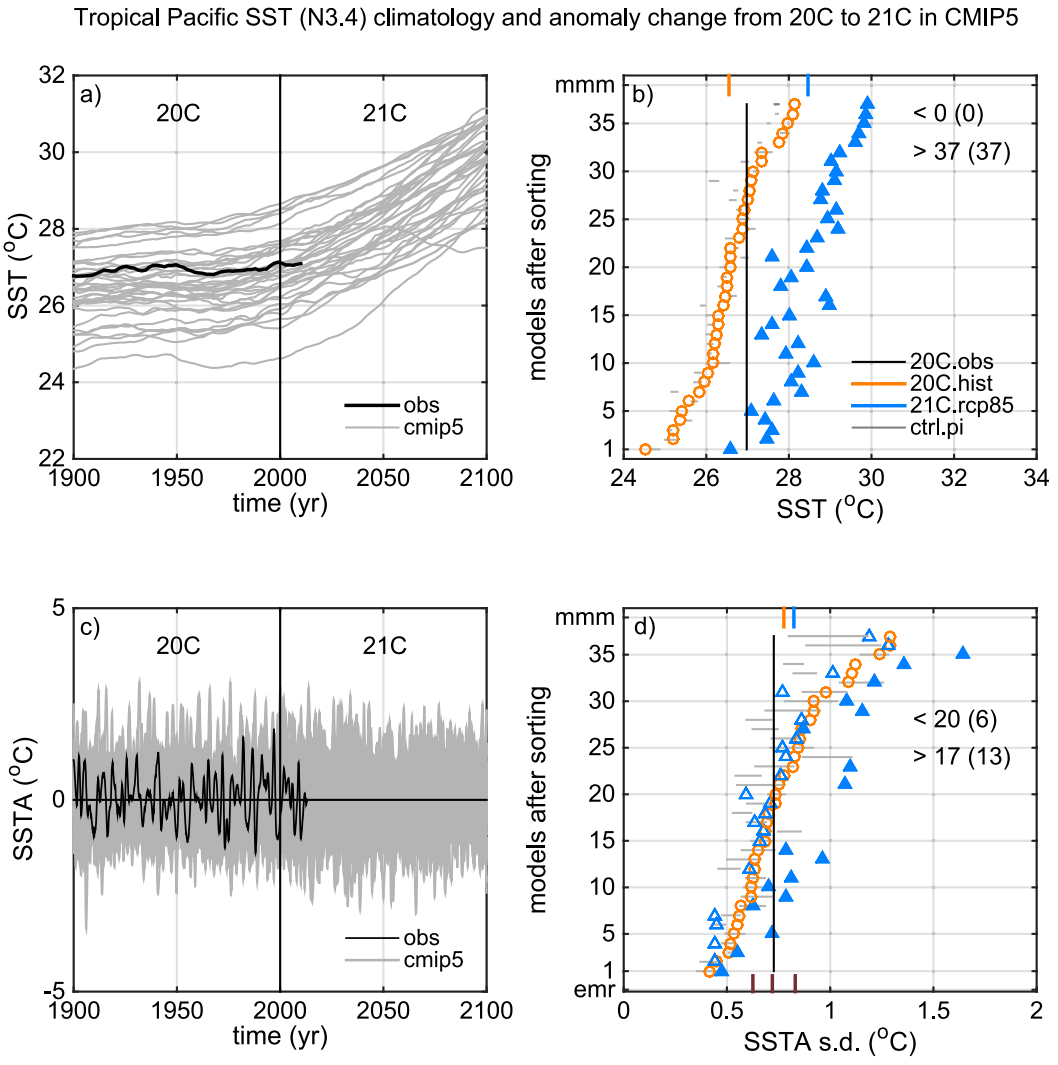

FIG. 9. Niño-3.4 SST climatology and anomaly in the twentieth century (20C, historical run, 1900–99) and the twenty-first century (21C, RCP8.5 scenario, 2000–99) in 37 CMIP5 models that participated in IPCC AR5. (a) The 20-yr running average Niño-3.4 SST with OBS in black and CMIP5 models in gray. (b) The mean SST in the 20C and 21C for each CMIP5 model. The models are sorted according to the 100-yr averaged Niño-3.4 SST in the 20C runs. The black vertical line marks the 20C OBS value. The multimodel mean (MMM) is shown at the top, with 20C in orange and 21C in blue. Preindustrial control simulations of each model are divided into 100-yr sliding epochs to calculate the 100-yr averaged SST and the 2.5th–97.5th percentile of the distribution are shown as gray horizontal lines. The number of models with decreased (<) / increased (>) change is indicated in (b) and (d). The number in the brackets is the count for significant changes out of the range given by the control run. (c) Niño-3.4 SST anomaly time series from 1900 to 2099. (d) The standard deviation of SSTA in preindustrial, 20C, and 21C runs. In addition here the 21C results with an increased change are shown filled and those with decreased values are unfilled. Meanwhile, the 2.5th, 50th, 97.5th percentile range estimated from the distribution in the EMR simulation is shown in brown vertical bars at the bottom.

The natural variation range is provided by PI control runs of each model and the 4000-yr stochastic-forced EMR simulation fit from OBS. The MMM for 20C overestimates the ENSO amplitude. There is large spread ranging from half the amplitude of OBS to nearly twice, consistent with the findings in Bellenger et al. (2014). For the 21C, the MMM of 37 models projects an increase in Niño-3.4 s.d.; 20 (17) models show a decrease (an increase), among which 6 (13) models are significant.

b. SST annual cycle and seasonality

The annual cycle of 20C Niño-3.4 SST of all CMIP5 models are presented in Fig. 10a. The structure of the annual cycle is measured using an index I_{seacli} defined as

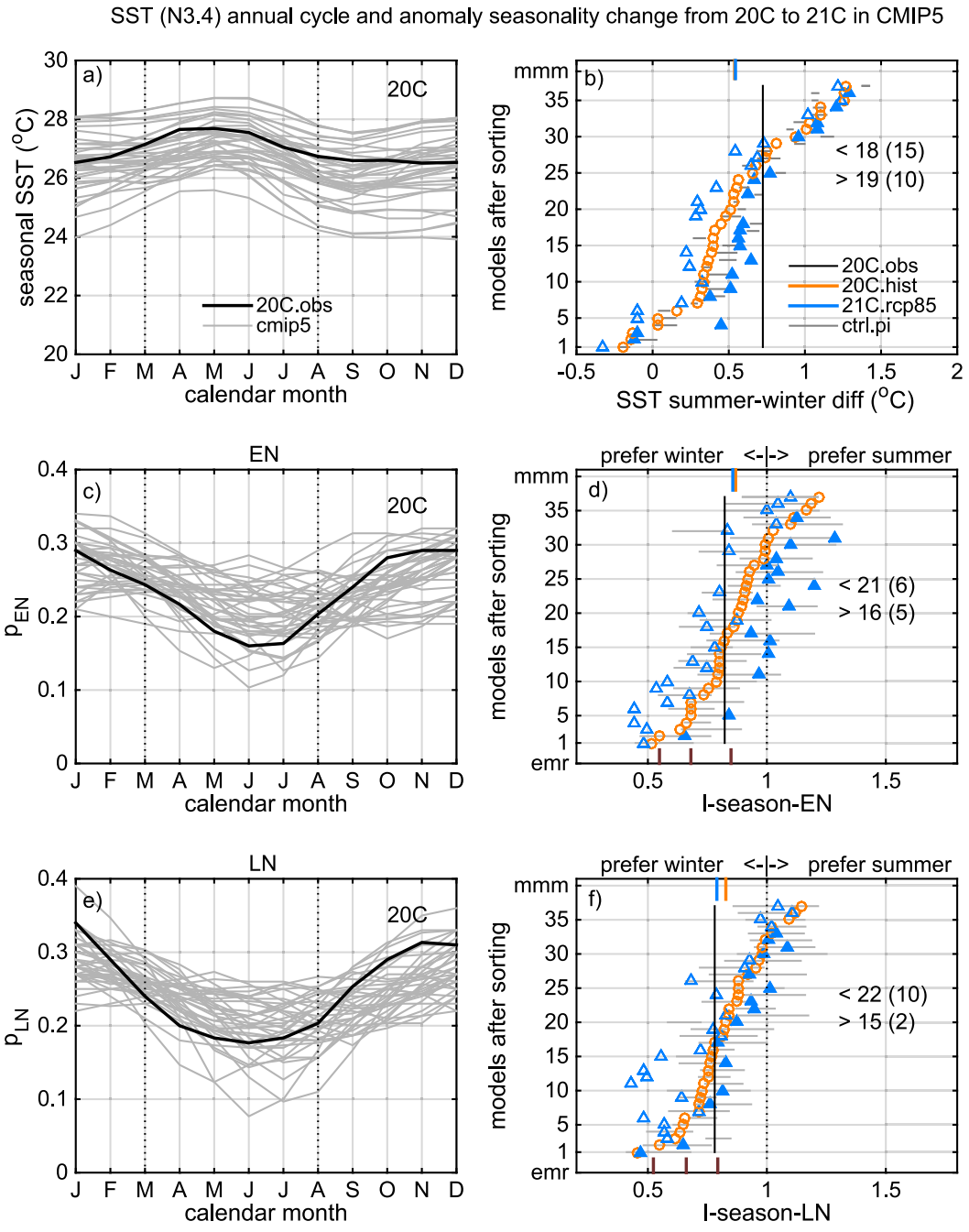

FIG. 10. Annual cycle and ENSO seasonality change from the twentieth century (20C) to twenty-first century (21C) in 37 CMIP5 models. (a) The 20C seasonal cycle of Niño-3.4 SST, with OBS in black and CMIP5 models in gray. The horizontal axis shows the calendar month. (b) The Niño-3.4 SST difference between the March–August (summer half year) average and the September–February (winter half year) average. The models are sorted according to the 20C value of this difference. (c),(e) 20C occurrence probability of El Niño P_{EN} and La Niña P_{LN}, respectively. (d) Seasonality index of El Niño ($I_{season-EN}$) defined using summer half year averaged P_{EN} divided by winter half year averaged P_{EN}; thus, $I_{season-EN} < 1$ indicates that El Niño in a given 100-yr epoch prefers winter phase locking. (f) $I_{season-LN}$, defined the same way, but for La Niña event.

the averaged SST during winter half year (September–February) minus that during summer half year (March–August). Most models produce a reasonable annual cycle but some models show a semiannual cycle. MMM for 20C indicates a weaker annual cycle than observation. For 21C, MMM does not project an apparent change. It is found that 18 (19) models project a decrease (an increase), among which 15 (10) models are significant.

The seasonal phase locking for El Niño and La Niña is shown using occurrence probability for each calendar month (Figs. 10c,e). Most models produce a winter phase locking as in 20C OBS, consistent with Taschetto et al. (2014). But some models show no preferred peak season or peak in summer. Previous studies (e.g., Guilyardi et al. 2003; Ham and Kug 2014) suggested that the biased models in seasonality tend to also have biases in climatology and oceanic mean state. The seasonal locking for El Niño and La Niña measured by I_{sea} is shown in Figs. 10d and 10f. Although there is large spread among models, MMM for 20C appears to overall match the observation. For 21C, MMM does not project much change for El Niño and only a slight change for La Niña. For El Niños, 21 (16) models project a decrease (an increase), among which 6 (5) models are significant. For La Ninas, 22 (15) models project a decrease (increase), among which 15 (2) models are significant.

c. *ENSO diversity in peak location*

For the 20C simulation, 37 models show a large spread for the ratio between CP and EP ENSO $I_{cp/ep}$ (Figs. 11a,c). More than half of the models resemble the observation that El Niños favor the eastern Pacific although MMM slightly overestimates the value of $I_{cp/ep}$. More than half of the models resemble the observation in favoring La Niñas peaking at the central Pacific, although MMM slightly underestimates the value of $I_{cp/ep}$.

For the 21C projection, 20 (17) models project a decrease (an increase) for El Niños, among which 1 model is (2 models are) significant. For La Ninas, 15 (22) models project a decrease (an increase), among which 4 (5) models are significant. MMM results show no notable change. Yeh et al. (2009) analyzed 12 CMIP3 models in which an increased frequency of CPEN compared to EPEN is suggested to be related to the flattening of the thermocline in the equatorial Pacific. Kim and Yu (2012) analyzed 16 CMIP5 models under the RCP4.5 scenario that suggest an increased ratio of CP to EP El Niño. Taschetto et al. (2014) used 27 CMIP5 models under the RCP8.5 scenario that suggest no notable enhancement of the ratio of CP to EP ENSO. Here we analyzed 37 CMIP5 models in RCP8.5 scenario and measure the projected change from 20C to 21C using the probability shift of relative occurrence ($I_{cp/ep}$). The discrepancy among above studies suggests that the projections heavily depend on the selected models and the uncertainty is large given the varying performance of these models for the historical period.

d. *ENSO diversity in propagation direction*

For the 20C simulation, more than half of the models favor westward propagating El Niños as the observation although MMM overestimates the value of $I_{e/w}$ (Fig. 11b). Almost all models favor westward propagating La Niñas and MMM overall matches with the observations (Fig. 11d). For El Niños, 13 (24) models project a decrease (an increase), among which 2 (14) models are significant. For La Ninas, 12 (25) models project a decrease (an increase), among which 6 (15) models are significant. As suggested by Santoso et al. (2013), the projected weakening of the westward mean equatorial currents may explain the projected shift toward more eastward propagating El Niños and La Niñas in a warmer world.

e. *ENSO asymmetry in amplitude, duration, and transition*

The skewness of Niño-3.4 SST anomaly (Fig. 12a) coarsely measures the El Niño–La Niña asymmetry in amplitude, so it is discussed here together along with I_{amp}. For 20C, more than half of the 37 models show a positive sign of skewness in agreement with OBS, although MMM underestimates the value of skewness. For 21C, MMM shows a slight decrease of skewness; 24 (13) models project a decrease (an increase), among which 8 (2) models are significant.

The amplitude asymmetry I_{amp} (Fig. 12b) shows that more than half the models agree with OBS in 20C with larger amplitude in El Niño than in La Niña, although MMM underestimates the asymmetry. For 21C, MMM projects a decrease in the asymmetry; 21 (16) models project a decrease (an increase), among which 7 (3) models are significant. The duration asymmetry I_{dur} (Fig. 11c) shows that only half the models agree with 20C OBS in showing a more persistent La Niña. MMM also underestimates the asymmetry. For 21C, MMM does not show much change; 16 (21) models project a decrease (an increase), among which 5 (2) models are significant. As to the transition I_{tra}, most models show much larger transition asymmetry than OBS in 20C and MMM also overestimates the asymmetry. For 21C, MMM does not show much change; 19 (18) models project a decrease (an increase), among which 3 (5) models are significant. For all three aspects of EN–LN asymmetry, the projected changes are largely within the natural variation range based upon the control run.

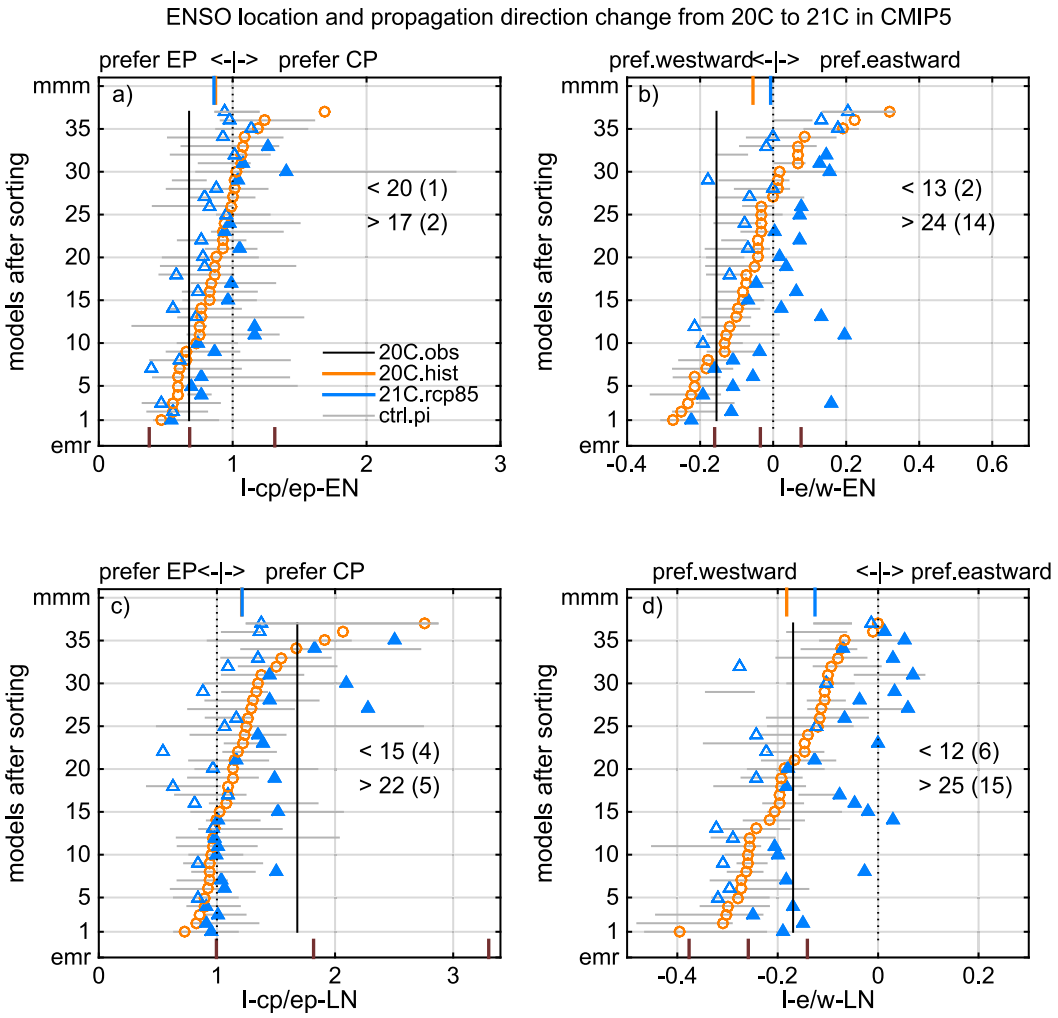

FIG. 11. ENSO peaking location and propagation direction in the twentieth century (20C) and twenty-first century (21C) in 37 CMIP5 models. (a) The location diversity index $I_{cp/ep}$ for EN, defined as P_{CPEN} divided by P_{EPEN}. (c) $I_{cp/ep}$ for LN. $I_{cp/ep} > 1$ indicates El Niños or La Niñas preferentially peak in CP. (b) The propagation diversity index $I_{e/w}$ for EN. (d) $I_{e/w}$ for La Niña. $I_{e/w} > 0$ indicates El Niños or La Niñas prefer eastward propagation.

Previous studies (e.g., Zhang and Sun 2014; Cai et al. 2015a) pointed out that most CMIP5 models underestimate the ENSO asymmetry. Here the results in our diagnostics show that, among these three aspects, the EN–LN asymmetry in amplitude and duration are underestimated by most models, and the EN–LN asymmetry in transition is usually overestimated.

6. Discussion

a. Which aspect may show a robust change in 21C?

Now we would like to summarize, among all the ENSO behaviors we have analyzed in this study, which aspects may show a robust change in 21C. Increasing SST climatology, as the result of changing external forcing, is consistently predicted by all models. Other than that, changes in many SSTA aspects are not that robust, and the differences between 20C and 21C are largely within the range of the natural variation.

We first estimate which aspects are most responsive to the trend forcing, in which case the changes could be readily detected from the natural variation in the model projection. For each aspect, we count the number of models (denoted as N_c) out of 37 models showing a significant change (no matter positive or negative changes). The results are as follows: SST climatology ($N_c = 37$), annual cyle I_{seacli} ($N_c = 25$), standard deviation of Niño-3.4 ($N_c = 19$), diversity in zonal propagation for El Niño $I_{e/w-EN}$ ($N_c = 16$) and La Niña $I_{e/w-LN}$ ($N_c = 21$), seasonality of El Niño I_{sea-EN} ($N_c = 11$) and La Niña I_{sea-LN} ($N_c = 12$), the EN–LN asymmetry in I_{amp} ($N_c = 10$), I_{dur} ($N_c = 7$), I_{tra} ($N_c = 8$), and diversity in

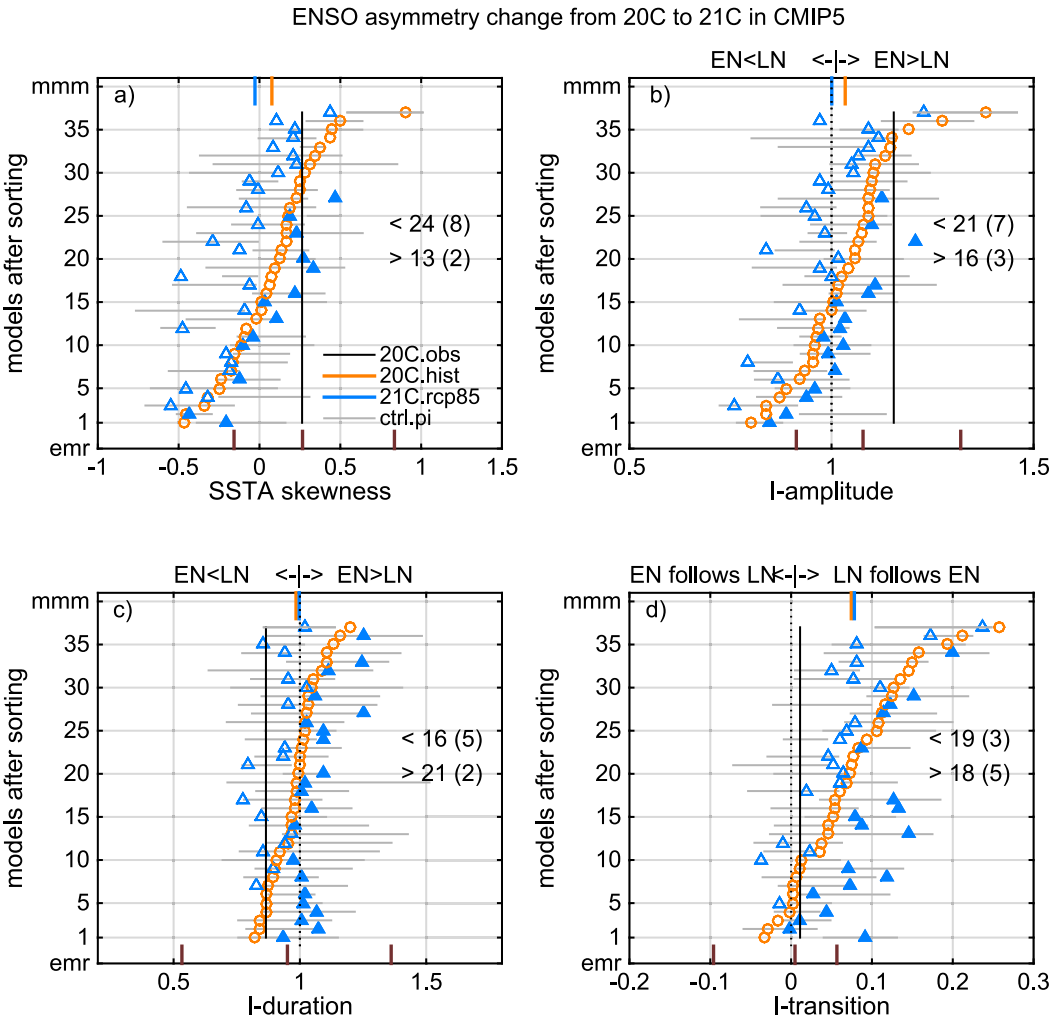

FIG. 12. EN–LN asymmetry in the twentieth century (20C) and twenty-first century (21C) in 37 CMIP5 models. (a) The skewness of Niño-3.4 SSTA. (b) The amplitude asymmetry index (I_{amp}) defined as EN amplitude divided by LN amplitude. $I_{amp} > 1$ indicates El Niños have larger amplitude than La Niñas in a given 100-yr epoch. (c) The duration asymmetry index (I_{dur}). $I_{dur} < 1$ indicates La Niñas are more persistent than El Niños. (d) The transition asymmetry index (I_{tra}). $I_{tra} > 0$ indicates El Niños are quickly followed by La Niñas but not vice versa.

peak location for El Niño $I_{cp/ep-EN}$ ($N_c = 3$) and La Niña $I_{cp/ep-LN}$ ($N_c = 9$).

Among these 12 aspects, SST climatology gives $N_c = 37$, suggesting that SST mean state quickly adjusts to the increasing greenhouse gas emissions so that all 37 models can readily capture this change. However, diversity in peak location $I_{cp/ep}$ only gives $N_c = 3$ for El Niño and $N_c = 9$ for La Niña. It suggests that El Niño peaking at eastern Pacific or central Pacific often varies even under a constant forcing. Therefore the large range of natural variation makes it difficult to detect the forced response.

Although the change of the annual cycle is very responsive to forcing ($N_c = 25$), 37 models still do not give a clear direction of change [18 (19) models show a decrease (an increase), among which 15 (10) models show a significant decrease/increase]. Therefore, it is difficult to argue whether the annual cycle would become weaker in the twenty-first century.

The change of the standard deviation of Niño-3.4 is also very responsive to forcing ($N_c = 19$); 20 (17) models project a decrease (an increase), among which 6 (13) models project a significant decrease/increase. L. Chen et al. (2015) investigated the physical mechanisms for four individual models showing either increasing or decreasing ENSO amplitude in the warming climate. The authors found that models with a stronger (weaker) equatorial thermocline response to the zonal wind anomaly tend to project a strengthened (weakened) ENSO amplitude.

A shift toward eastward propagation of El Niños and La Niñas is the responsive aspect with the most robust change supported by MMM and nearly two-thirds of the models. Santoso et al. (2013) have shown that the westward mean current is one main reason for ENSO's westward propagation. Therefore a shift toward favoring the eastward propagating El Niño may be the response to the weakened westward mean current as projected for 21C.

By basing our metrics on SSTA we follow the practice in the vast majority of prior ENSO literature. However, based on observations (Karl et al. 1995), CMIP modeling results, and theory (Allen and Ingram 2002), it is expected that with global warming the atmospheric water vapor content will increase along with the intensifying convective events. Thus we expect that the rainfall associated with ENSO events will increase, as has been found by Power et al. (2013), Cai et al. (2014), and Cai et al. (2015b).

b. *Projection using a subset of models*

Studies of CMIP models often identify subsets of good models based on various metrics (e.g., Gleckler et al. 2008; Kim and Yu 2012; Bellenger et al. 2014). In this study, we would like to estimate if a subset of good models may give a more reliable projection for 21C with a better model agreement. Here we identify good models based on 13 aspects of ENSO behavior. Table 1 summarizes 37 CMIP5 model performances based on these 13 metrics. For each aspect, 10 models with the smallest errors in 20C are marked with an asterisk. We then use the total number of asterisks to identify the overall best 10 models. After that, we summarize the model performance in 20C and the projection for 21C using the MMM of all 37 models, the overall best 10 models (b10), and the best 10 models for individual aspect (c10) (Fig. 13). Skewness is not shown in this summary since it is closely correlated with EN–LN asymmetry in amplitude.

We note that the MMM using the subset of good models is closer to the 20C observation for each aspect, but the future projection based on these models still lacks consensus for most aspects. It is possible that 1) the external forcing for 21C may be implemented slightly differently in each individual model and 2) model dynamics are slightly different in each model so that they may drive different responses even under the same forcing. Therefore one needs to be cautious for the future projection even using a subset of "good" models.

c. *ENSO behavior biases in CMIP5 models*

Compared to the 20C observation, 37-model mean results (a37 in Fig. 13) show the CMIP5 model biases are reflected in many aspects (e.g., underestimated mean SST, overly weak annual cycle, overly strong SST variability, more CPEN and EPLN, more eastward propagating EN, underestimated EN–LN asymmetry in amplitude and duration, and excessive asymmetry in transition).

Do the biases in ENSO behavior have some relation with the biases in the simulated mean state of Niño-3.4? Figure 14 displays the results for PI, 20C, and 21C. Note that the scatterplot shows the overall spread when 37 Earth-like systems respond given the same forcing. It may not be interpreted as a physical relation, since it does not come from one consistent system under a series of different mean states. For example, Fig. 13b shows that, among all 37 models, models that simulate a relatively warmer mean state tend to also simulate a weak annual cycle with a small summer–winter difference in SST. But this apparent relation may not suggest that the annual cycle will become weaker in the warming climate. The previous section already showed that the change of the annual cycle from 20C to 21C varies in each individual model and the MMM shows no significant change.

7. Conclusions

We introduced a set of empirical probabilistic diagnostics for ENSO behaviors, including variations in peak season, location, and propagation direction as well as El Niño–La Niña asymmetries. The diagnostics applied to SST observations show that El Niños and La Niñas are phase-locked to boreal winter. They both favor westward propagation. El Niños mainly occur at the eastern Pacific and La Niñas prefer the central Pacific. These results agree with current understanding and thus provide support for the validity of our new diagnostics.

The diagnostics were applied to evaluate ENSO behaviors in two example simulations. The first is a 4000-yr preindustrial control simulation of the GFDL CM2.1 coupled GCM. The strong nonlinearity of this model is indicated by an exaggerated El Niño–La Niña asymmetry. Although modeled La Niñas generally behave like the observations, El Niños behave quite differently. El Niño's winter phase-locking feature is largely missed since eastern Pacific El Niños (EPENs) prefer peaking in summer while central Pacific El Niños (CPENs) prefer winter. Eastward propagating El Niños are dominant. The overall statistics are largely dominated by extreme El Niños.

The diagnostics were also applied to a 4000-yr stochastic-forced simulation of a nonlinear empirical model reduction (EMR) fit using SST observations. This simulation is reasonably realistic in broad aspects of ENSO behavior and thus may be considered as an extension to observations to help us assess the range of

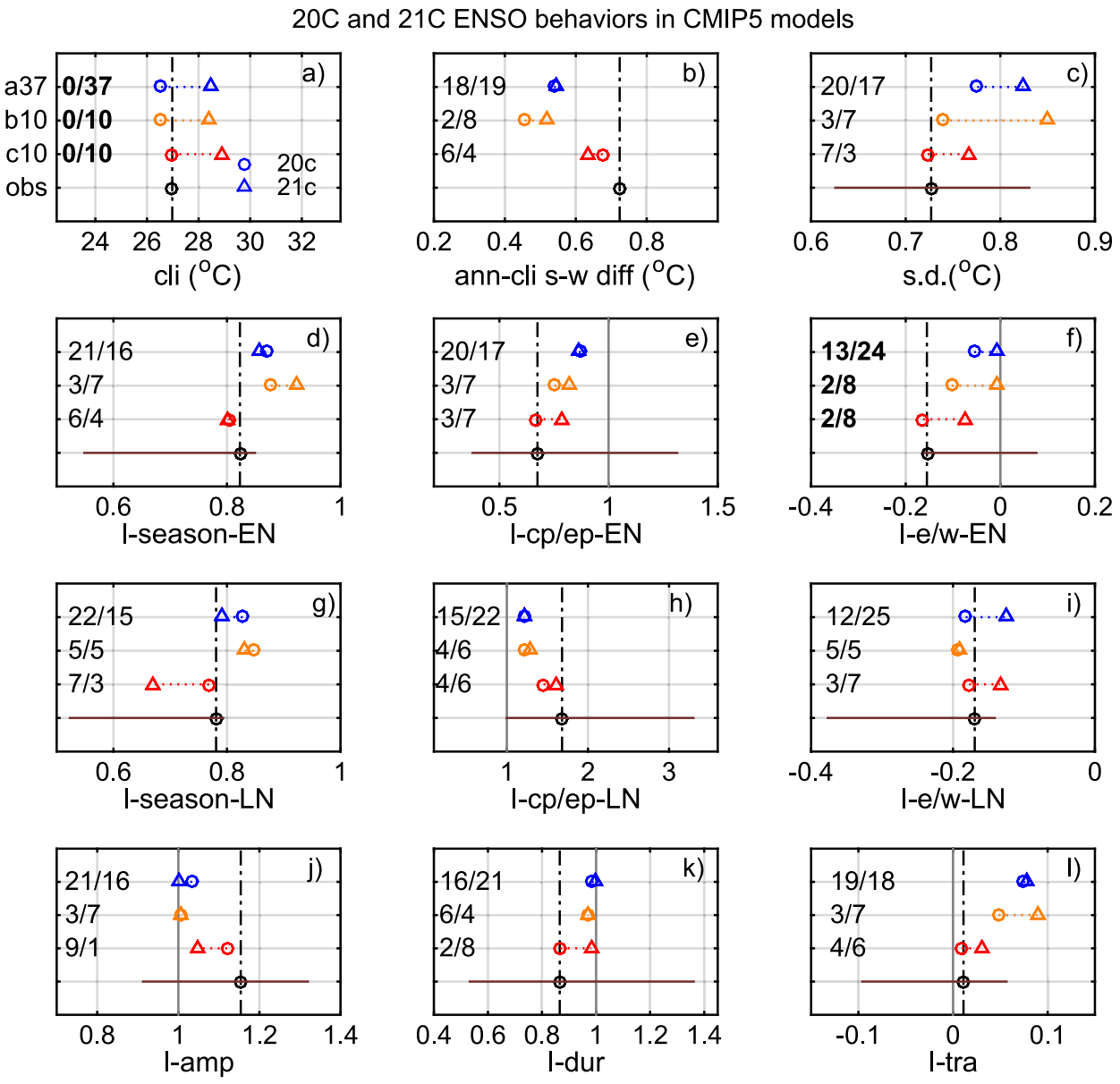

FIG. 13. Summary of ENSO behaviors in the twentieth century and the twenty-first century using all 37 CMIP5 models (a37, blue), overall best 10 models (b10, yellow) and best 10 models for individual aspect of behavior (c10, red). The twentieth-century observation (obs, black) results are shown as a reference. A 4000-yr stochastically forced simulation of EMR model fit from the observation provides the natural variation range (the 2.5–97.5 percentile range is shown). In each panel, a pair of numbers indicates the degree of model agreement. The left one is the number of models showing a decrease from the twentieth century to the twenty-first century while the right one is the number of models showing an increase.

ENSO variation. Most epochs in a 4000-yr simulation agree well with observations. But epochs with more CP El Niños or epochs with more eastward El Niños do exist when stochastic noise is the only forcing. No forcing trend such as that due to greenhouse gases is required.

The diagnostics were then applied to assess the potential change of ENSO behaviors in a warming climate using 37 CMIP5 models that participated in IPCC AR5. Evaluation of model performance used twentieth-century runs (20C, historical, 1900–99) show that each model has pros and cons for varying aspects of ENSO behavior.

As for the projected changes from the twentieth century to twenty-first century (21C, RCP8.5 scenario, 2000–99), except for a consensus in tropical Pacific SST increase due to the forcing, changes in other aspects are

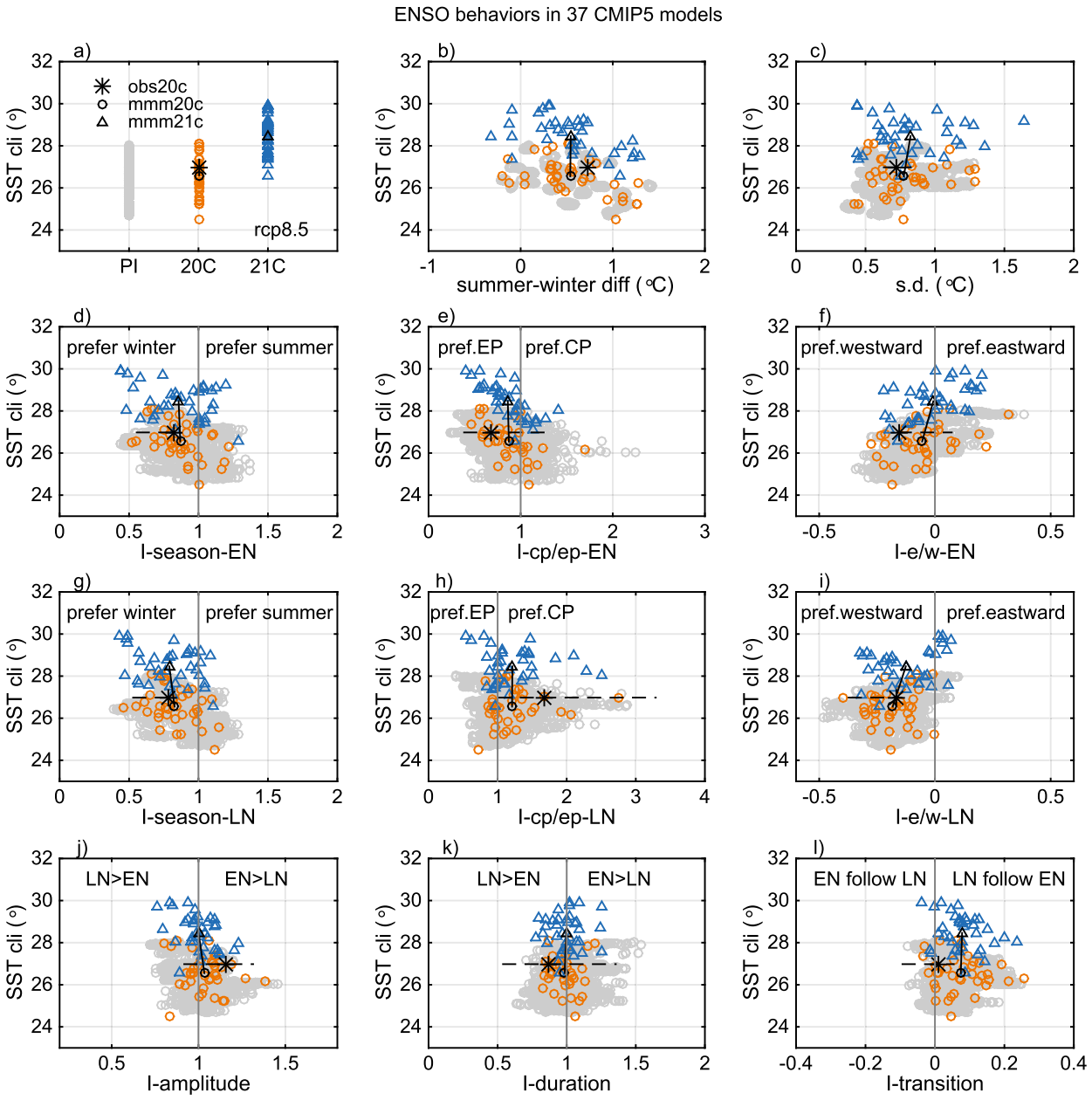

FIG. 14. ENSO behaviors biases in CMIP5 models. (a) The Niño-3.4 SST climatology in each model for the preindustrial period (PI; gray circle), the twentieth century (20C; orange circle) to the twenty-first century (21C; (blue triangle). 20C observations are indicated with an asterisk. (b)–(l) Each individual ENSO behavior varies at different mean states. The change from 20C MMM to 21C MMM is shown with a black line. The 2.5th–97.5th percentiles of natural variation range by EMR are shown by dashed lines.

all model dependent. Except for the warming climatology, many 21C changes are within the bounds of the natural variation range produced by the preindustrial control runs (PI) control run. Overall the multimodel mean (MMM) suggests that changes in many ENSO statistics measured in SSTA may not be significant (e.g., diversity peaking in eastern Pacific–central Pacific and El Niño–La Niña asymmetries). Although a few models do show significant changes, the degree of model agreement on the projected change is low for all aspects. A shift favoring eastward propagating El Niño and La Niña shows slightly more robustness.

Projections for the future based on CMIP models often involve considerable uncertainty (Vecchi and Wittenberg 2010). Changes in ENSO are difficult to detect given large natural variability present in each

model (e.g., Wittenberg 2009) as well as the lack of model agreement (e.g., Guilyardi 2006; Collins et al. 2010; Stevenson 2012; Taschetto et al. 2014). In this study, various model biases for 20C ENSO behaviors leave little to confidently predict the future of ENSO. Whether the projected changes could actually take place in the future remains largely uncertain. The ENSO behavior diagnostics introduced in this study and data-driven models (e.g., EMR) fit from the observation may be useful along with the development of CMIP models.

Acknowledgments. We thank Dong Eun Lee, Naomi Henderson, and David Chapman for inspiring discussions and Haibo Liu for archiving the CMIP5 data at LDEO. We also thank three anonymous reviewers for their helpful comments. This study is supported by the Office of Naval Research under the research grant MURI (N00014-12-1-0911). DC also acknowledges grants from the National Basic Research Program (2013CB430302), the National Natural Science Foundation of China (41321004, 91128204), and the IPOVAR Project. We acknowledge the World Climate Research Programme's Working Group on Coupled Modelling, which is responsible for CMIP, and we thank the climate modeling groups (listed in Table 1 of this paper) for producing and making available their model output. For CMIP the U.S. Department of Energy's Program for Climate Model Diagnosis and Intercomparison provides coordinating support and led development of software infrastructure in partnership with the Global Organization for Earth System Science Portals.

APPENDIX

EMR Methodology

Empirical model reduction (EMR) is an empirical modeling framework, allowing nonlinearity, seasonality, and memory effects (Kravtsov et al. 2005; Kondrashov et al. 2005, 2015). The operational version of EMR (labeled UCLA-TCD) participates in the International Research Institute for Climate and Society's (IRI's) ENSO prediction plume, and it is very competitive among both dynamical and statistical models (Barnston et al. 2012; http://iri.columbia.edu/our-expertise/climate/forecasts/enso/current/).

The setting of EMR used in this study is as follows. The state vector $\mathbf{x} = \{x_i\}$ is the leading three normalized PCs of detrended tropical Pacific SSTA. Quadratic nonlinearity is included in the main level:

$$dx_i = (\mathbf{x}^T \mathbf{A}_i \mathbf{x} + \mathbf{b}_i^1 \mathbf{x} + c_i^1)dt + dr_i^1; \quad i = 1, \ldots, 3. \tag{A1}$$

The model coefficients in matrices $\mathbf{A}_i$, the vectors $\mathbf{b}_i$ of matrix $\mathbf{B}$, the components c_i of vector $\mathbf{c}$, and the components r_i of the residual $\mathbf{r}$ are determined by multiple polynomial regression.

Seasonality is included by adding additional coefficients into the main level of the model:

$$\mathbf{B} = \mathbf{B}_n + \mathbf{B}_s \sin(2\pi t/T) + \mathbf{B}_c \cos(2\pi t/T), \tag{A2}$$

$$\mathbf{c} = \mathbf{c}_n + \mathbf{c}_s \sin(2\pi t/T) + \mathbf{c}_c \cos(2\pi t/T), \tag{A3}$$

where the matrix $\mathbf{B}_n$ and vector $\mathbf{c}_n$ are the original annually averaged (nonseasonal) terms as in Eq. (A1), matrices $\mathbf{B}_s$ and $\mathbf{B}_c$ add an multiplicative seasonality, and vectors $\mathbf{c}_s$ and $\mathbf{c}_c$ add an additive seasonality. The period $T = 12$ months to account for an annual cycle of seasonality. All these coefficients are determined simultaneously with the other coefficients in the main level.

The ENSO memory effect is embedded in a two-time-level model construction. An additional level is added by fitting the temporal increment of the residual at the main level $d\mathbf{r}^1$ using a linear function of an extended state vector $[\mathbf{x}, \mathbf{r}^1]$:

$$dr_i^1 = \mathbf{b}_i^2[\mathbf{x}, \mathbf{r}^1]dt + dr_i^2; \quad i = 1, \ldots, 3, \tag{A4}$$

where $\mathbf{b}_i^2$ and r_i^2 for the second level (i.e., one time step back) are determined after the main level. Results from Kondrashov et al. (2005) and Chen et al. (2016) indicate that two time levels are sufficient to embed a memory effect for ENSO simulation. A stochastic simulation is forced using a spatially coherent multivariate white noise given by the residual covariance matrix estimated along with the model fitting. See more details in Kondrashov et al. (2005).

In this study, EMR uses the same setting as the model 2L+S+NL in Chen et al. (2016), which is a nonlinear model with two time levels and an annual seasonality. To investigate the dependence of ENSO behaviors on the system nonlinearity, we also construct a linear model denoted EMR-L for a comparison. It uses the same setting as the model 2L+S in Chen et al. (2016), which has two time levels and an annual seasonality. The only difference between EMR and EMR-L is with or without nonlinearity.

REFERENCES

Allen, M. R., and W. J. Ingram, 2002: Constraints on future changes in climate and the hydrologic cycle. *Nature*, **419**, 224–232, doi:10.1038/nature01092.

An, S.-I., and B. Wang, 2001: Mechanisms of locking of the El Niño and La Niña mature phases to boreal winter. *J. Climate*, **14**, 2164–2176, doi:10.1175/1520-0442(2001)014<2164:MOLOTE>2.0.CO;2.

——, and F.-F. Jin, 2004: Nonlinearity and asymmetry of ENSO. *J. Climate*, **17**, 2399–2412, doi:10.1175/1520-0442(2004)017<2399:NAAOE>2.0.CO;2.

Ashok, K., S. K. Behera, S. A. Rao, H. Weng, and T. Yamagata, 2007: El Niño Modoki and its possible teleconnection. *J. Geophys. Res.*, **112**, C11007, doi:10.1029/2006JC003798.

Barnston, A. G., M. K. Tippett, M. L. L'Heureux, S. Li, and D. G. DeWitt, 2012: Skill of real-time seasonal ENSO model predictions during 2002–11: Is our capability increasing? *Bull. Amer. Meteor. Soc.*, **93**, 631–651, doi:10.1175/BAMS-D-11-00111.1.

Bellenger, H., E. Guilyardi, J. Leloup, M. Lengaigne, and J. Vialard, 2014: ENSO representation in climate models: From CMIP3 to CMIP5. *Climate Dyn.*, **42**, 1999–2018, doi:10.1007/s00382-013-1783-z.

Cai, W., and Coauthors, 2014: Increasing frequency of extreme El Niño events due to greenhouse warming. *Nat. Climate Change*, **4**, 111–116, doi:10.1038/nclimate2100.

——, and Coauthors, 2015a: ENSO and greenhouse warming. *Nat. Climate Change*, **5**, 849–859, doi:10.1038/nclimate2743.

——, and Coauthors, 2015b: Increased frequency of extreme La Niña events under greenhouse warming. *Nat. Climate Change*, **5**, 132–137, doi:10.1038/nclimate2492.

Cane, M. A., S. E. Zebiak, and Y. Xue, 1995: Model studies of the long-term behavior of ENSO. *Natural Climate Variability on Decade-to-Century Time Scales*, D. G. Martinson et al., Eds., National Academies Press, 442–457.

——, A. C. Clement, A. Kaplan, Y. Kushnir, D. Pozdnyakov, R. Seager, S. E. Zebiak, and R. Murtugudde, 1997: Twentieth-century sea surface temperature trends. *Science*, **275**, 957–960, doi:10.1126/science.275.5302.957.

Capotondi, A., A. Wittenberg, and S. Masina, 2006: Spatial and temporal structure of Tropical Pacific interannual variability in 20th century coupled simulations. *Ocean Modell.*, **15**, 274–298, doi:10.1016/j.ocemod.2006.02.004.

——, and Coauthors, 2015: Understanding ENSO diversity. *Bull. Amer. Meteor. Soc.*, **96**, 921–938, doi:10.1175/BAMS-D-13-00117.1.

Chen, C., M. A. Cane, N. Henderson, D. E. Lee, D. Chapman, D. Kondrashov, and M. D. Chekroun, 2016: Diversity, nonlinearity, seasonality, and memory effect in ENSO simulation and prediction using empirical model reduction. *J. Climate*, **29**, 1809–1830, doi:10.1175/JCLI-D-15-0372.1.

Chen, D., and Coauthors, 2015: Strong influence of westerly wind bursts on El Niño diversity. *Nat. Geosci.*, **8**, 339–345, doi:10.1038/ngeo2399.

Chen, L., T. Li, and Y. Yu, 2015: Causes of strengthening and weakening of ENSO amplitude under global warming in four CMIP5 models. *J. Climate*, **28**, 3250–3274, doi:10.1175/JCLI-D-14-00439.1.

Choi, K.-Y., G. A. Vecchi, and A. T. Wittenberg, 2013: ENSO transition, duration, and amplitude asymmetries: Role of the nonlinear wind stress coupling in a conceptual model. *J. Climate*, **26**, 9462–9476, doi:10.1175/JCLI-D-13-00045.1.

Clement, A. C., R. Seager, M. A. Cane, and S. E. Zebiak, 1996: An ocean dynamical thermostat. *J. Climate*, **9**, 2190–2196, doi:10.1175/1520-0442(1996)009<2190:AODT>2.0.CO;2.

Collins, M., and Coauthors, 2010: The impact of global warming on the tropical Pacific Ocean and El Niño. *Nat. Geosci.*, **3**, 391–397, doi:10.1038/ngeo868.

Delworth, T. L., and Coauthors, 2006: GFDL's CM2 global coupled climate models. Part I: Formulation and simulation characteristics. *J. Climate*, **19**, 643–674, doi:10.1175/JCLI3629.1.

DiNezio, P. N., and C. Deser, 2014: Nonlinear controls on the persistence of La Niña. *J. Climate*, **27**, 7335–7355, doi:10.1175/JCLI-D-14-00033.1.

Dommenget, D., T. Bayr, and C. Frauen, 2013: Analysis of the nonlinearity in the pattern and time evolution of El Niño Southern Oscillation. *Climate Dyn.*, **40**, 2825–2847, doi:10.1007/s00382-012-1475-0.

Fedorov, A. V., and S. G. Philander, 2001: A stability analysis of tropical ocean–atmosphere interactions: Bridging measurements and theory for El Niño. *J. Climate*, **14**, 3086–3101, doi:10.1175/1520-0442(2001)014<3086:ASAOTO>2.0.CO;2.

——, S. Hu, M. Lengaigne, and E. Guilyardi, 2015: The impact of westerly wind bursts and ocean initial state on the development and diversity of El Niño events. *Climate Dyn.*, **44**, 1381–1401, doi:10.1007/s00382-014-2126-4.

Frauen, C., and D. Dommenget, 2010: El Niño and La Niña amplitude asymmetry caused by atmospheric feedbacks. *Geophys. Res. Lett.*, **37**, L18801, doi:10.1029/2010GL044444.

Gleckler, P. J., K. E. Taylor, and C. Doutriaux, 2008: Performance metrics for climate models. *J. Geophys. Res.*, **113**, D06104, doi:10.1029/2007JD008972.

Guilyardi, E., 2006: El Niño–mean state–seasonal cycle interactions in a multi-model ensemble. *Climate Dyn.*, **26**, 329–348, doi:10.1007/s00382-005-0084-6.

——, P. Delecluse, S. Gualdi, and A. Navarra, 2003: Mechanisms for ENSO phase change in a coupled GCM. *J. Climate*, **16**, 1141–1158, doi:10.1175/1520-0442(2003)16<1141:MFEPCI>2.0.CO;2.

——, A. Wittenberg, A. Fedorov, M. Collins, C. Wang, A. Capotondi, G. J. van Oldenborgh, and T. Stockdale, 2009: Understanding El Niño in ocean–atmosphere general circulation models: Progress and challenges. *Bull. Amer. Meteor. Soc.*, **90**, 325–340, doi:10.1175/2008BAMS2387.1.

——, W. Cai, M. Collins, A. Fedorov, F.-F. Jin, A. Kumar, D.-Z. Sun, and A. Wittenberg, 2012: New strategies for evaluating ENSO processes in climate models. *Bull. Amer. Meteor. Soc.*, **93**, 235–238, doi:10.1175/BAMS-D-11-00106.1.

Ham, Y.-G., and J.-S. Kug, 2012: How well do current climate models simulate two types of El Nino? *Climate Dyn.*, **39**, 383–398, doi:10.1007/s00382-011-1157-3.

——, and ——, 2014: ENSO phase-locking to the boreal winter in CMIP3 and CMIP5 models. *Climate Dyn.*, **43**, 305–318, doi:10.1007/s00382-014-2064-1.

Hirahara, S., M. Ishii, and Y. Fukuda, 2014: Centennial-scale sea surface temperature analysis and its uncertainty. *J. Climate*, **27**, 57–75, doi:10.1175/JCLI-D-12-00837.1.

Kang, I.-S., and J.-S. Kug, 2002: El Niño and La Niña sea surface temperature anomalies: Asymmetry characteristics associated with their wind stress anomalies. *J. Geophys. Res.*, **107**, 4372, doi:10.1029/2001JD000393.

Kao, H.-Y., and J.-Y. Yu, 2009: Contrasting eastern-Pacific and central-Pacific types of ENSO. *J. Climate*, **22**, 615–632, doi:10.1175/2008JCLI2309.1.

Karamperidou, C., M. A. Cane, U. Lall, and A. T. Wittenberg, 2014: Intrinsic modulation of ENSO predictability viewed through a local Lyapunov lens. *Climate Dyn.*, **42**, 253–270, doi:10.1007/s00382-013-1759-z.

Karl, T. R., R. W. Knight, and N. Plummer, 1995: Trends in high-frequency climate variability in the twentieth century. *Nature*, **377**, 217–220, doi:10.1038/377217a0.

Karnauskas, K. B., 2013: Can we distinguish canonical El Niño from Modoki? *Geophys. Res. Lett.*, **40**, 5246–5251, doi:10.1002/grl.51007.

Kim, S. T., and J.-Y. Yu, 2012: The two types of ENSO in CMIP5 models. *Geophys. Res. Lett.*, **39**, L11704, doi:10.1029/2012GL052006.

Kim, W., and W. Cai, 2014: The importance of the eastward zonal current for generating extreme El Niño. *Climate Dyn.*, **42**, 3005–3014, doi:10.1007/s00382-013-1792-y.

Kondrashov, D., S. Kravtsov, A. W. Robertson, and M. Ghil, 2005: A hierarchy of data-based ENSO models. *J. Climate*, **18**, 4425–4444, doi:10.1175/JCLI3567.1.

——, M. D. Chekroun, and M. Ghil, 2015: Data-driven non-Markovian closure models. *Physica D*, **297**, 33–55, doi:10.1016/j.physd.2014.12.005.

Kravtsov, S., D. Kondrashov, and M. Ghil, 2005: Multilevel regression modeling of nonlinear processes: Derivation and applications to climatic variability. *J. Climate*, **18**, 4404–4424, doi:10.1175/JCLI3544.1.

Kug, J.-S., and Y.-G. Ham, 2011: Are there two types of La Nina? *Geophys. Res. Lett.*, **38**, L16704, doi:10.1029/2011GL048237.

——, F.-F. Jin, and S.-I. An, 2009: Two types of El Niño events: Cold tongue El Niño and warm pool El Niño. *J. Climate*, **22**, 1499–1515, doi:10.1175/2008JCLI2624.1.

——, J. Choi, S.-I. An, F.-F. Jin, and A. T. Wittenberg, 2010: Warm pool and cold tongue El Niño events as simulated by the GFDL 2.1 coupled GCM. *J. Climate*, **23**, 1226–1239, doi:10.1175/2009JCLI3293.1.

Larkin, N., and D. Harrison, 2002: ENSO warm (El Niño) and cold (La Niña) event life cycles: Ocean surface anomaly patterns, their symmetries, asymmetries, and implications. *J. Climate*, **15**, 1118–1140, doi:10.1175/1520-0442(2002)015<1118:EWENOA>2.0.CO;2.

——, and ——, 2005: On the definition of El Niño and associated seasonal average U.S. weather anomalies. *Geophys. Res. Lett.*, **32**, L13705, doi:10.1029/2005GL022738.

Lee, S.-K., A. T. Wittenberg, D. B. Enfield, S. J. Weaver, C. Wang, and R. Atlas, 2016: US regional tornado outbreaks and their links to spring ENSO phases and North Atlantic SST variability. *Environ. Res. Lett.*, **11**, 044008, doi:10.1088/1748-9326/11/4/044008.

Lee, T., and M. J. McPhaden, 2010: Increasing intensity of El Niño in the central-equatorial Pacific. *Geophys. Res. Lett.*, **37**, L14603, doi:10.1029/2010GL044007.

Lengaigne, M., and G. A. Vecchi, 2010: Contrasting the termination of moderate and extreme El Niño events in coupled general circulation models. *Climate Dyn.*, **35**, 299–313, doi:10.1007/s00382-009-0562-3.

Levine, A. F. Z., and F.-F. Jin, 2016: A simple approach to quantifying the noise–ENSO interaction. Part I: Deducing the state-dependency of the windstress forcing using monthly mean data. *Climate Dyn.*, doi:10.1007/s00382-015-2748-1, in press.

McPhaden, M. J., and X. Zhang, 2009: Asymmetry in zonal phase propagation of ENSO sea surface temperature anomalies. *Geophys. Res. Lett.*, **36**, L13703, doi:10.1029/2009GL038774.

Neelin, J. D., F.-F. Jin, and H.-H. Syu, 2000: Variations in ENSO phase locking. *J. Climate*, **13**, 2570–2590, doi:10.1175/1520-0442(2000)013<2570:VIEPL>2.0.CO;2.

Newman, M., S.-I. Shin, and M. Alexander, 2011: Natural variation in ENSO flavors. *Geophys. Res. Lett.*, **38**, L14705, doi:10.1029/2011GL047658.

Ohba, M., and H. Ueda, 2009: Role of nonlinear atmospheric response to SST on the asymmetric transition process of ENSO. *J. Climate*, **22**, 177–192, doi:10.1175/2008JCLI2334.1.

Okumura, Y. M., M. Ohba, C. Deser, and H. Ueda, 2011: A proposed mechanism for the asymmetric duration of El Niño and La Niña. *J. Climate*, **24**, 3822–3829, doi:10.1175/2011JCLI3999.1.

Power, S., F. Delage, C. Chung, G. Kociuba, and K. Keay, 2013: Robust twenty-first-century projections of El Niño and related precipitation variability. *Nature*, **502**, 541–545, doi:10.1038/nature12580.

Rayner, N. A., D. E. Parker, E. B. Horton, C. Folland, L. V. Alexander, D. P. Rowell, E. C. Kent, and A. Kaplan, 2003: Global analyses of sea surface temperature, sea ice, and night marine air temperature since the late nineteenth century. *J. Geophys. Res.*, **108**, 4407, doi:10.1029/2002JD002670.

Santoso, A., S. McGregor, F.-F. Jin, W. Cai, M. H. England, S.-I. An, M. J. McPhaden, and E. Guilyardi, 2013: Late-twentieth-century emergence of the El Niño propagation asymmetry and future projections. *Nature*, **504**, 126–130, doi:10.1038/nature12683.

Schopf, P., and R. Burgman, 2006: A simple mechanism for ENSO residuals and asymmetry. *J. Climate*, **19**, 3167–3179, doi:10.1175/JCLI3765.1.

Solomon, A., and M. Newman, 2012: Reconciling disparate twentieth-century Indo-Pacific ocean temperature trends in the instrumental record. *Nat. Climate Change*, **2**, 691–699, doi:10.1038/nclimate1591.

Stein, K., N. Schneider, A. Timmermann, and F.-F. Jin, 2010: Seasonal synchronization of ENSO events in a linear stochastic model. *J. Climate*, **23**, 5629–5643, doi:10.1175/2010JCLI3292.1.

Stevenson, S., 2012: Significant changes to ENSO strength and impacts in the twenty-first century: Results from CMIP5. *Geophys. Res. Lett.*, **39**, L17703, doi:10.1029/2012GL052759.

——, B. Fox-Kemper, M. Jochum, R. Neale, C. Deser, and G. Meehl, 2012: Will there be a significant change to El Niño in the twenty-first century? *J. Climate*, **25**, 2129–2145, doi:10.1175/JCLI-D-11-00252.1.

Takahashi, K., and B. Dewitte, 2016: Strong and moderate nonlinear El Niño regimes. *Climate Dyn.*, **46**, 1627–1645, doi:10.1007/s00382-015-2665-3.

——, A. Montecinos, K. Goubanova, and B. Dewitte, 2011: ENSO regimes: Reinterpreting the canonical and Modoki El Niño. *Geophys. Res. Lett.*, **38**, L10704, doi:10.1029/2011GL047364.

Taschetto, A. S., and M. H. England, 2009: El Niño Modoki impacts on Australian rainfall. *J. Climate*, **22**, 3167–3174, doi:10.1175/2008JCLI2589.1.

——, A. Sen Gupta, N. C. Jourdain, A. Santoso, C. C. Ummenhofer, and M. H. England, 2014: Cold tongue and warm pool ENSO events in CMIP5: Mean state and future projections. *J. Climate*, **27**, 2861–2885, doi:10.1175/JCLI-D-13-00437.1.

Taylor, K. E., R. J. Stouffer, and G. A. Meehl, 2012: An overview of CMIP5 and the experiment design. *Bull. Amer. Meteor. Soc.*, **93**, 485–498, doi:10.1175/BAMS-D-11-00094.1.

Tziperman, E., M. A. Cane, and S. E. Zebiak, 1995: Irregularity and locking to the seasonal cycle in an ENSO prediction model as explained by the quasi-periodicity route to chaos. *J. Atmos. Sci.*, **52**, 293–306, doi:10.1175/1520-0469(1995)052<0293:IALTTS>2.0.CO;2.

——, S. E. Zebiak, and M. A. Cane, 1997: Mechanisms of seasonal–ENSO interaction. *J. Atmos. Sci.*, **54**, 61–71, doi:10.1175/1520-0469(1997)054<0061:MOSEI>2.0.CO;2.

——, M. A. Cane, S. E. Zebiak, Y. Xue, and B. Blumenthal, 1998: Locking of El Niño's peak time to the end of the calendar year in

the delayed oscillator picture of ENSO. *J. Climate*, **11**, 2191–2199, doi:10.1175/1520-0442(1998)011<2191:LOENOS>2.0.CO;2.

Vecchi, G. A., and A. T. Wittenberg, 2010: El Niño and our future climate: Where do we stand? *Wiley Interdiscip. Rev.: Climate Change*, **1**, 260–270, doi:10.1002/wcc.33.

Weng, H., K. Ashok, S. K. Behera, S. A. Rao, and T. Yamagata, 2007: Impacts of recent El Niño Modoki on dry/wet conditions in the Pacific rim during boreal summer. *Climate Dyn.*, **29**, 113–129, doi:10.1007/s00382-007-0234-0.

Wittenberg, A. T., 2009: Are historical records sufficient to constrain ENSO simulations? *Geophys. Res. Lett.*, **36**, L12702, doi:10.1029/2009GL038710.

——, A. Rosati, N.-C. Lau, and J. J. Ploshay, 2006: GFDL's CM2 global coupled climate models. Part III: Tropical Pacific climate and ENSO. *J. Climate*, **19**, 698–722, doi:10.1175/JCLI3631.1.

——, ——, T. L. Delworth, G. A. Vecchi, and F. Zeng, 2014: ENSO modulation: Is it decadally predictable? *J. Climate*, **27**, 2667–2681, doi:10.1175/JCLI-D-13-00577.1.

Xiao, H., and C. R. Mechoso, 2009: Seasonal cycle–El Niño relationship: Validation of hypotheses. *J. Atmos. Sci.*, **66**, 1633–1653, doi:10.1175/2008JAS2870.1.

Xie, S.-P., C. Deser, G. A. Vecchi, J. Ma, H. Teng, and A. T. Wittenberg, 2010: Global warming pattern formation: Sea surface temperature and rainfall. *J. Climate*, **23**, 966–986, doi:10.1175/2009JCLI3329.1.

Yeh, S.-W., J.-S. Kug, B. Dewitte, M.-H. Kwon, B. P. Kirtman, and F.-F. Jin, 2009: El Niño in a changing climate. *Nature*, **461**, 511–514, doi:10.1038/nature08316.

——, B. P. Kirtman, J.-S. Kug, W. Park, and M. Latif, 2011: Natural variability of the central Pacific El Niño event on multicentennial timescales. *Geophys. Res. Lett.*, **38**, L02704, doi:10.1029/2010GL045886.

Yu, J.-Y., and S. T. Kim, 2010: Identification of Central-Pacific and Eastern-Pacific types of ENSO in CMIP3 models. *Geophys. Res. Lett.*, **37**, L15705, doi:10.1029/2010GL044082.

——, Y. Zou, S. T. Kim, and T. Lee, 2012: The changing impact of El Niño on US winter temperatures. *Geophys. Res. Lett.*, **39**, L15702, doi:10.1029/2012GL052483.

Zebiak, S. E., and M. A. Cane, 1987: A model El Niño–Southern Oscillation. *Mon. Wea. Rev.*, **115**, 2262–2278, doi:10.1175/1520-0493(1987)115<2262:AMENO>2.0.CO;2.

Zhang, T., and D.-Z. Sun, 2014: ENSO asymmetry in CMIP5 models. *J. Climate*, **27**, 4070–4093, doi:10.1175/JCLI-D-13-00454.1.